Irrigation with Bavaria water

The optimal drain water level and the temperature effects of subirrigation with treated wastewater in Aarle Rixtel

Janneke Pouwels

April 5, 2017

Irrigation with Bavaria water

The optimal drain water level and the temperature effects of subirrigation with treated wastewater in Aarle Rixtel

Janneke Pouwels

April 5, 2017

MSc thesis report

Supervisors:

Dr. Ir. J.C. van Dam

Soil Physics and Land Management
Wageningen University & Research

Dr. Ir. R.P. Bartholomeus

Ecohydrology
KWR Watercycle Research

Abstract

The last decade the groundwater table in the Netherlands was reduced. Without adaptation measures this reduction will continue in the future, largely caused by climate change. The reduction of the groundwater table causes a decrease in the soil moisture content, which may cause a decrease in crop yield. One way to improve the soil moisture conditions for agriculture is by using subirrigation. Subirrigation is irrigation where the water is pumped into the field through underground drains. There the irrigation water will directly increase the soil moisture content in the rooting zone. The subirrigation water is first collected in a collection well. From the collection well, the water will flow through the drains and will eventually reach the soil. The irrigation flux is determined by the hydraulic head of the irrigation water in the drains, which is regulated by the water level in the supply well. At this moment an experiment is going on in the south of the Netherlands where treated restwater from the Bavaria brewery is used as subirrigation water. In this research it is investigated what the optimal hydraulic head is of this irrigation water, in order to limit drought stress and achieve the highest crop yield. Hereby scenarios of three crop types are used: grass, maize and potatoes. For grass it is also investigated what the optimal irrigation head is with climate change. The investigated optimal irrigation heads are higher for grass than for maize and potatoes, Besides, the optimal irrigation heads become higher in the future, due to climate change. The subirrigation causes a reduction in the drought stress and therefore causes an increase in yield of 3.5% for grass. For potatoes and maize, this increase in yield is much lower. Next to the optimal head, the effect of the relatively warm irrigation water on the soil temperature is investigated. The soil temperature near the drain is significant higher than the soil temperature further away from the drain, at a depth of 40 and 60 cm. This temperature increase may lead to an extend in the growing season. Due to the higher crop yields and the extension of the growing season caused by subirrigation, it can be concluded that the reuse of process water for subirrigation of grass is useful, because the subirrigation with process water will cause a larger crop yield. In the future the subirrigation with process water will increase the yield even more. Therefore it is recommended to reuse process water for subirrigation on more locations in the Netherlands.

Contents

Chapter 1

Introduction

1.1 General introduction

The Netherlands is a small and relatively flat country which mainly consists of deltas. A significant part (26%) of the land is located below sea level (Planbureau voor de Leefomgeving, 2007). Due to the relatively flatness and low lying of the country, the groundwater table can be found within a few meters below soil surface. This is also because the Netherlands has an overall excess in precipitation. Only in the summer there is a precipitation shortage. The available water in the Netherlands is used for different purposes. The water is used as domestic water, it is incorporated in products, it is used temporary (e.g. as industrial cooling water) and it is used to create desired conditions of water levels and water quality. The water quality can be improved by flushing areas with a poor water quality. A large part of the water incorporated in products is used in the agricultural sector. In this sector precipitation water is in the summer not enough to meet the water requirements. Also in other parts of the year the precipitation water may not be enough for some crop types. This water shortage can cause a decrease in crop yield. Sometimes irrigation is used to increase the water availability and to keep a high crop yield (Klijn *et al.*, 2011).

The groundwater level affects the availability of soil moisture through capillary rise. Herewith, the groundwater level is an important variable in the agricultural sector and plays a major role in the maximum possible crop yield. If the groundwater level is too shallow or too deep, without irrigation crops will suffer from dry or wet stress. This will reduce the crop yield (Moene & Van Dam, 2014). The groundwater level is subject to changes by climate change. Climate change plays a role by altering the sea level, the average temperature, the average precipitation and the precip-

itation variability (Kundzewicz & Döll, 2009). All these variables form complex relations, through which it is difficult to predict the influence of climate change on the groundwater level. Next to climate change, urbanisation has its impact on the groundwater level. Urbanization reduces the groundwater recharge because precipitation will immediately flow to the sewer system (Kundzewicz & Döll, 2009). The groundwater level is also lowering because of groundwater extraction. The extracted water is mostly used by the industry and the agricultural sector (CBS *et al.*, 2016). Most of the extracted water does not return to the groundwater, because it is eventually discharged to the surface water. Altogether, climate change, urbanisation and groundwater extraction are the main drivers for the lowering in the groundwater table in the last decades. This lowering of groundwater levels causes a decrease in water availability and hence an increase in drought stress experienced by crops. Therefore the crop yield will decrease if no adaption measures are taken. To prevent decreasing crop yields, the soil moisture should be increased. This can be done by several irrigation techniques. This research focuses on raising the groundwater level through subsurface irrigation through drainage systems (subirrigation).

1.2 Research objective

The groundwater table can be increased by using subirrigation. Subirrigation is irrigation through underground drains, where the water comes from a collection pipe through drains in the soil. The subirrigation causes a local increase in the groundwater level, as can be seen in figure 1.1. Due to the adaptable water level in the collection pipe and therefore adaptable hydraulic head inside the drains, the water will infiltrate into the soil. By using industrial process water for subirrigation, extracted industrial water will eventually return to the soil and will recharge the groundwater. Besides, when subirrigation is used, conventional (aboveground) irrigation may not be necessary anymore. Therefore groundwater extraction by the agricultural sector will decrease. These measures together will decrease the current lowering of the groundwater table and lower the pressure on the groundwater.

Currently the Dutch Bavaria Beer Brewery, located in Lieshout, puts a lot of effort in a sustainable beer production. The brewery uses a lot of groundwater in the production process. To become more sustainable, the Bavaria Brewery wants to contribute to the decrease of the current water shortage by reusing its process water

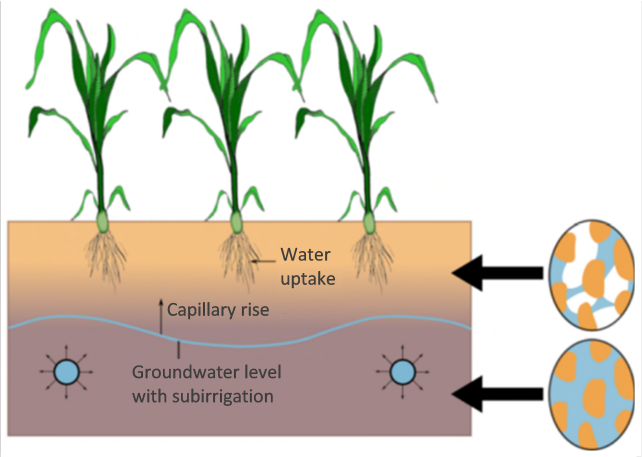

Figure 1.1: An overview of subirrigation. The subirrigation causes a local highering of the groundwater level. From Bartholomeus & van Loon (2017).

as subirrigation water. Nearby farmers are enthusiastic about this initiative. At this moment, research institute KWR is investigating the technical and economic feasibility of the reuse of Bavaria wastewater for subirrigation. This research focuses on the effect of subirrigation on the water quality and the water balance of the surrounding area. For this research, at one farmer field in Aarle Rixtel (from now on called 'study area') subirrigation is already implemented. The irrigation water is about 20°C, depending on the season, and comes from the nearby Bavaria Beer Brewery.

It is not yet investigated what hydraulic head and which amounts of water are needed in the drains in order to get the highest crop yield. If groundwater levels could be raised such that the soil moisture availability in the root zone increases, subirrigation causes a reduction in drought stress by crops. On the other hand, the groundwater level and soil moisture content should not be too high because crops can also suffer from waterlogging stress. Therefore it is important to investigate the best head inside the drains in order to have the highest crop yield. Already a lot of research is done on subirrigation. Research mostly focuses on the working of the water table control and the differences in costs, plant health and erosion in comparison with other irrigation methods (Dukes *et al.*, 2010; Kacimov & Obnosov, 2016; Kazumba *et al.*, 2010). The optimal irrigation head is hypothesized to be time, crop and soil specific. Therefore using head values from literature will not lead to the highest possible crop yield in the study area. Hence, for achieving the highest possible crop yield, it is necessary to investigate the optimal irrigation

head in the study area.

The temperature of the irrigation water, which is about 20°C as it leaves the Bavaria factory, can have its influence on the crop growth. Research has shown that the crop growth approximately linearly increases with increasing temperature (Hunt *et al.*, 1985a). Both the air temperature and the soil temperature contribute to the environmental temperature of crops. Therefore it is hypothesized that the warmer irrigation water may cause an extension of the growing season and therefore maybe cause an increase in crop yield. The exact influence of the temperature of irrigation water is not yet known. To test this hypothesis, the effect of the irrigation water on the soil temperature and the effect of the soil temperature on the crop growth should be investigated. Due to limited time, only the effect of the irrigation water on the soil temperature will be investigated in this research.

Consequently, more knowledge on temperature effects and drainage levels are needed to optimize the moisture conditions by subirrigation in the study area. Therefore, the following research questions can be formulated:

- What is the optimal subirrigation water head in the study area to achieve the highest crop yield?
- To which extent does the soil temperature change due to the subirrigation?

To answer these questions it is important to fully understand the atmosphere-vegetation-soil system and how it is influenced by the subirrigation. Not only the current system should be understood, but also how the system reacts to changes. Therefore different scenarios are used to answer the research questions.

First of all the influence of climate change on the research questions will be investigated. In here the four climate scenarios of the KNMI (Gl, Gh, Wl and Wh, Klein Tank *et al.* (2015)) will be used for the year 2050. These climate scenarios vary in the amount of temperature increase and the change in the air flow pattern. Climate scenarios Gl and Gh will have a temperature increase of 1°C and Wl and Wh of 2°C in 2050, compared to the climate 1981-2010. Climate scenarios Gl and Wl will have a small change in the air flow pattern and scenarios Wl and Wh will have a large change in the air flow pattern at 2050, compared to the climate 1981-2010. In all climate scenarios the winter precipitation increases and the intensity of the summer precipitation increases (Klein Tank *et al.*, 2015). Next to climate change, the impact of changing crop types will be

investigated. Currently, the crop type is grass. In two scenarios the growth of maize and potatoes at the study area will be investigated. While grass is a perennial species, maize and potatoes are annual species.

Altogether, the following scenarios are formulated:

- The current situation in the study area;
- The situation of the year 2050, taking climate change into account;
- The change of crop types from grass to potatoes;
- The change of crop types from grass to maize.

The research questions will be answered for every scenario, by making use of a SWAP-WOFOST model of the study area. Besides, measurements of soil temperature, groundwater level and soil moisture are used. The soil moisture characteristics and hydraulic conductivity function will be measured in the soil physical laboratory. The SWAP-WOFOST model will be explained in paragraph 4.3.

Chapter 2

Theoretical framework

Knowledge on processes in the atmosphere-vegetation-soil system is needed before answering the research questions. Therefore this chapter gives a review on the known processes in and links between atmosphere, vegetation and soil. Besides, a review is given on the recent research on subirrigation.

2.1 Transport processes in the soil

For understanding the heat and water balance between atmosphere, crops and soil, it is important to understand how heat and water are transported in the soil. Therefore this section describes both water transport and heat transport inside the soil.

2.1.1 Water transport

Soil water flows mainly vertically in the unsaturated zone and mainly horizontally in the saturated zone. When using the assumption that soil layers, root densities and boundary conditions are horizontally uniform, flow in the unsaturated zone can be seen as fully vertical. The application of Darcy's law about soil water flow for vertical flow reads:

$$q = -K(h)\frac{\partial(h+z)}{\partial z} \tag{2.1}$$

With q is the water flux [cm d^{-1}], K is the unsaturated hydraulic conductivity [cm d^{-1}], h is the hydraulic head [cm] and z is the vertical coordinate [cm] (positive upward).

When looking at an infinitely small volume, a mass balance can be made for the soil water:

$$\frac{\partial\theta}{\partial t} = -\frac{\partial q}{\partial z} - S_a(h) - S_d(h) - S_m(h) \tag{2.2}$$

In which θ is the soil water content [cm^3 cm^{-3}], t is time [d], S_a is the soil water extraction by plant roots [cm^3 cm^{-3} d^{-1}], S_d is the water extraction by drains [cm^3 cm^{-3} d^{-1}] and S_m is the exchange by macropores [cm^3 cm^{-3} d^{-1}]. The mass balance and Darcy's equation can be combined to the Richards equation (Richards, 1931), which is the general water flow equation in the saturated zone. It reads:

$$\frac{\partial \theta}{\partial t} = \frac{\partial \left[K(h)\left(\frac{\partial h}{\partial z} + 1\right)\right]}{\partial z} - S_a(h) - S_d(h) - S_m(h) \tag{2.3}$$

Soil water flow in the unsaturated zone can be described by soil hydraulic functions. Widely used functions are the analytical Mualem - van Genuchten functions. In here the soil hydraulic conductivity is described by the soil water retention function (van Genuchten, 1980):

$$\theta(h) = \theta_{res} + \frac{\theta_{sat} - \theta_{res}}{(1 + (\alpha h)^n)^m} \tag{2.4}$$

Where θ_{res} is the residual water content [cm^3 cm^{-3}], θ_{sat} is the saturated water content [cm^3 cm^{-3}] and α [m^{-1}], n [-] and m [-] are shape parameters. Without losing much flexibility, m can be related to n in: $m = 1 - \frac{1}{n}$.

The hydraulic conductivity is described by (van Genuchten, 1980):

$$K = K_{sat} S_e^{\lambda} \left[1 - \left(1 - S_e^{\frac{1}{m}}\right)^m\right]^2 \tag{2.5}$$

With K_{sat} is the saturated hydraulic conductivity [cm d^{-1}], λ is a shape parameter [-] and S_e is the relative saturation [-], defined by:

$$S_e = \frac{\theta - \theta_{res}}{\theta_{sat} - \theta_{res}} \tag{2.6}$$

The parameters θ_{res}, θ_{sat}, α, n, m, K_{sat} and λ are called 'the van Genuchten parameters'. By using the Mualem - van Genuchten functions, care should be taken that small changes in the pF curve near saturation can cause significant changes in hydraulic conductivity (Vogel *et al.*, 2000).

2.1.2 Heat transport

The soil temperature is determined by the density of the soil heat flux. The soil heat flux due to conduction can be expressed as (Kroes *et al.*, 2008):

$$q_{heat} = -\lambda_{heat} \frac{\partial T}{\partial z} \tag{2.7}$$

Where q_{heat} is the soil heat flux [J cm^{-2} d^{-1}], λ_{heat} is the thermal conductivity [J cm^{-1} °C^{-1} d^{-1}] and T is the temperature [°C]. Conservation of energy can be expressed as (Kroes *et al.*, 2008):

$$C_{heat}\frac{\partial T}{\partial t} = \frac{-\partial q_{heat}}{\partial z} \tag{2.8}$$

Where C_{heat} is the soil heat capacity [J cm^{-3} °C^{-1}]. Combining the heat transport with the conservation of energy results in the differential equation for soil heat flow:

$$C_{heat}\frac{\partial T}{\partial t} = \frac{\partial\left(\lambda_{heat}\frac{\partial T}{\partial z}\right)}{\partial z} \tag{2.9}$$

So the soil heat flux is related to the local temperature gradient and the thermal conductivity. Local temperature gradients can be caused by the diurnal temperature cycle. The thermal conductivity of soil and water is much higher than that of air. Therefore, a more saturated soil has a higher conductivity. Thermal conductivity is temperature dependent, due to the temperature dependency of the saturated vapour pressure. Another factor that can change the soil heat flux density is the transport of water. Therefore, the groundwater flux and groundwater temperature have its effect on the soil heat flux. This implies that the flux and the temperature of the irrigation water contributes to the soil heat flux (Moene & Van Dam, 2014).

2.2 Plant physiology

The water and heat transport in the soil will have its effect on crop growth. To further understand this effect, it is important to have some in-depth knowledge on plant physiology.

2.2.1 Basic plant growth

Crops use global radiation for their photosynthesis. Only 50% of the global radiation is photosynthetically active radiation (PAR). Part of this PAR is reflected by the crop leaves. The reflection can be described by (Goudriaan, 1977):

$$\rho_{rad} = \left(\frac{1-\sqrt{1-\sigma_{leaf}}}{1+\sqrt{1-\sigma_{leaf}}}\right)\left(\frac{2}{1+1.6\sin\beta_{sun}}\right) \tag{2.10}$$

With ρ_{rad} is the reflection coefficient [-], σ_{leaf} is the scattering coefficient of single leaves [-] and β_{sun} is the solar elevation [°]. The rate

of light adsorption can be described by:

$$PAR_{L,a} = \kappa\,(1 - \rho_{rad})\,PARe^{-\kappa L} \tag{2.11}$$

Where $PAR_{L,a}$ is the rate of light adsorption at a certain depth [J m^{-2} d^{-1}], L is the cumulative Leaf Area Index (LAI) counted from the top of the canopy to the specified depth [m^2 m^{-2}] and κ is the radiation extinction coefficient [-], which can be separated into a direct and a diffuse extinction coefficient.

By photosynthesis, the absorbed light is used to assimilate CO_2 to carbohydrates. From these carbohydrates, 15-30% is used for maintenance respiration, dependent on the dry weight of the structures (Penning de Vries & van Laar, 1982). The remaining carbohydrates are used for growth respiration. Over a wide range of temperatures, the crop growth is linearly related to the temperature (Hunt *et al.*, 1985b).

2.2.2 Influence of water availability on plant growth

Water is essential for crop growth. It is a chemical agent for assimilation and respiration. Water is also used as transporter of salts and hormones. Besides, water gives shape and solidity to plant tissues. Water also has an important function in the thermal control of plants. It dampens the daily temperature fluctuations due to the high heat capacity of water and plants can cool due to water transpiration. The incoming and outgoing fluxes of water in plants are high; during a dry and windy summer day, the fluxes are fifteen times the dry weight of the plant (Ehlers & Goss, 2003).

Water enters the plant through the roots. When entering the plant, the water is transported through the cortex to enter the stele (Ehlers & Goss, 2003). The hydraulic resistance of the cortex is largely determined by the porosity of the cell membranes, which in turn depends on the cell respiration (Moene & Van Dam, 2014). Only 1% of the incoming water is used for photosynthesis. The rest of the water leaves the plant as transpiration water through stomata on the leaves. Next to the available amount of water in the soil, there are two resistances which determine the amount of transpiration. These resistances are the stomatal resistance and the boundary-layer resistance (Moene & Van Dam, 2014).

Plants experience stress when facing extreme wet or extreme dry conditions. When facing drought stress, injuries in morphological, chemical and physiological plant properties occur (Gong *et al.*, 2013). Long roots and a high root density do not necessarily mean that plants have a high drought tolerance. The reason for this is

that long dense roots do not always lead to a high water availability at critical crop stages. Both soil hydraulic resistances and hydraulic architecture are important aspects in drought stress. The root hydraulic architecture determines the preference sites of the root for water uptake. This is determined by the xylem vessel size, the quantity of root cells, the quantity of root cell files and the aquaporin activity (Doussan *et al.*, 2006; Vadez, 2014).

When facing waterlogging stress, there is not enough oxygen supply to the roots for aerobic ATP production (Shingaki-Wells *et al.*, 2014). The amount of oxygen in the soil is only partly determined by the water content. More important is the oxygen transportation rate by diffusion and the consumption rate of oxygen (Cook *et al.*, 2013). These rates depend on the soil temperature, the crop growth rate, the soil texture and the biological activity in the soil (Bartholomeus *et al.*, 2008).The higher microbial activity at waterlogging causes a production of toxic compounds. These toxic compounds increase the amount of stress by plants (Irfan *et al.*, 2010).

Waterlogging stress has several effects on plants. First of all, oxidative phosphorylation no longer generates enough ATP (the storage molecules for chemical energy). Therefore the plant changes to an anaerobe metabolism in order to keep enough energy (Douma *et al.*, 2012; Shingaki-Wells *et al.*, 2014). Besides, waterlogging stress causes turgor loss, which accelerates leaf senescence (Wang *et al.*, 2016; Irfan *et al.*, 2010). The stress also induces fermentation and glycolysis. Light has its influence on the amount of waterlogging stress. The induce of fermentation is less in light than in the dark. Besides, nitrogen oxide and reactive oxygen species play important roles in waterlogging stress. Nitrate has a role in maintaining the redox balance and reactive oxygen species are produced when facing waterlogging conditions (Shingaki-Wells *et al.*, 2014). Reactive oxygen species may lead to mutations. Furthermore, flooding causes a direct closure of stomata. This results in a decrease in the exchange of foliar gas. Hence the internal CO_2-concentration rises. This causes a reduction in photosynthesis (Irfan *et al.*, 2010).

Almost all species can survive a short flooding, but only adapted plant species can survive longer periods of flood and also continue to produce seeds. Rice species are adapted to waterlogging circumstances. Rice can even germinate under anoxic (no oxygen) circumstances. Besides, ATP production of rice is reduced to only 25% of its production in aerobic circumstances. For non-adapted species, there is almost no ATP produced under anoxic circumstances (Shingaki-Wells *et al.*, 2014). Rice species can keep this high amount of ATP production by their strategy to transport oxy-

gen from aerial parts of the plant to hypoxic (low oxygen level) or anoxic parts of the roots. Another strategy of adapted species is the air chambers inside the root cells. By this the plant provides itself with air (Irfan *et al.*, 2010).

2.2.3 Influence of soil temperature on plant growth

The soil temperature has its effect on plants. If the soil temperature is outside the comfort zone of the species, it has a negative influence on the development of plants, especially in the later stages of crop growth. The photosynthesis, nutrient uptake, pollen viability and the growth will then reduce (Wahid *et al.*, 2007; Nxawe *et al.*, 2010a).

On the other hand, optimal soil temperatures can increase seed production, earlier germination and reduce the time of dormancy, which is a large advantage for farming (Hyvönen, 2011; Batlla & Benech-Arnold, 2015). Plant phenology is the timing of periodic plant lifecycle events, such as emergence and the start of seed growth (Wahid *et al.*, 2007). The phenological development is usually described by the development stage D_s, which is 0 at emergence, 1 at flowering and 2 at maturity (Kroes *et al.*, 2008). Phenology is influenced by the cumulative temperature, solar radiation and water availability (Zhao *et al.*, 2013). The influence of temperature on plant phenology is complex. Higher temperatures cause larger development rates, increased leaf growth rates and a quicker turnover from assimilation into biomass (van Dobben, 1962; Seligman & van Keulen, 1987; Hunt *et al.*, 1985b; Causton & Venus, 1981; Kroes *et al.*, 2008). By contrast, higher temperatures cause shorter growing periods, larger maintenance costs and a shorter lifespan of leaves (Kaše & Čatský, 1984; Penning de Vries & van Laar, 1982; Kroes *et al.*, 2008). The overall effect of all these relations is earlier germination at higher temperatures. This can be seen at the current expedite in germination of 2.3-5.2 days per decade, caused by higher temperatures due to climate change (Parry *et al.*, 2007). Not only germination, but also plant growth is influenced by temperature. Low temperatures cause lower nutrient uptake and lower chlorophyll levels. Besides, stomata will be closed at a low temperature, which will cause a decrease in photosynthesis (Nxawe *et al.*, 2010b). The temperature for optimal growth is different for shoots and roots. On average the optimal air temperature is 20-25°C. In the Netherlands the average air temperature is below this optimal temperature.

The use of subirrigation could have its influence on phenology and plant growth due to changing soil temperatures and water availability. Warm irrigation water can cause quicker growth and plant

development. Especially for perennial grasses this effect would be significant. This enhances a longer grazing period and more mowing times (Phelan *et al.*, 2015; Gauly *et al.*, 2013). Figure 2.1 shows the expected increase in soil temperature due to subirrigation. The irrigation water may only be found in the middle between two drains at a certain depth, due to the downward flow caused by precipitation excess. Therefore the temperature increase between drains may only be minor.

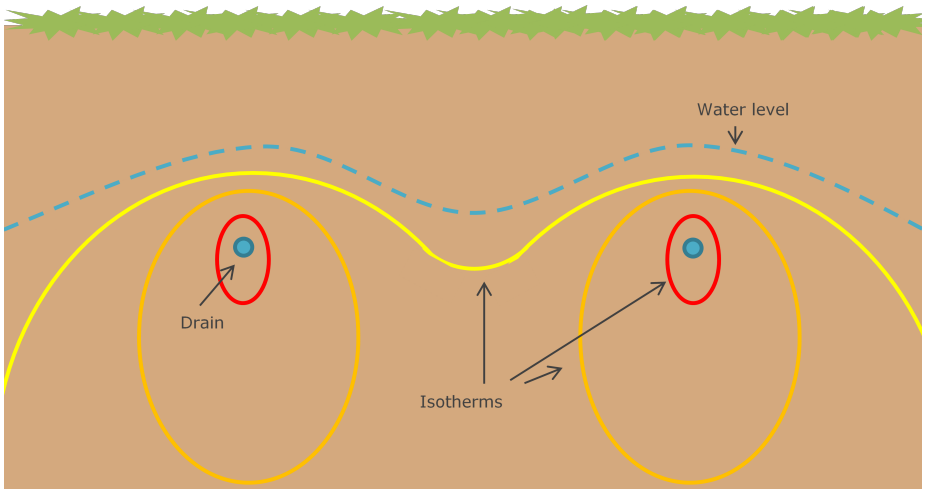

Figure 2.1: An overview of the water level and the temperature distribution when using subirrigation. The red isotherm is the isotherm with the highest temperature and the yellow isotherm is the isotherm with the lowest temperature.

2.3 Water balance

Crop growth is influenced by the water balance. On the other hand, the water balance is influenced by crop growth. Therefore the water balance will also be explained in this chapter.

2.3.1 Interception water

Precipitation and irrigation water are potential water sources for plants. Part of this water is interception water, which is caught by leaves and will evaporate again. Water which is not intercepted will infiltrate in the soil. Here the water can be absorbed by plant roots and eventually the water transpires. Interception and evapotranspiration play large roles in the water balance. So in order to know the

amount of soil moisture or the groundwater level, it is important to simulate these processes properly.

The total amount of precipitation is called gross precipitation and the precipitation which is infiltrated into the soil is called net precipitation. To describe the amount of interception water, Von Hoyningen Hüne and Brade used the formula (Braden, 1985; Von Hoyningen-Hüne, 1981):

$$P_i = a \cdot LAI \left(1 - \frac{1}{1 + \frac{b \cdot P_{gross}}{a \cdot LAI}} \right) \tag{2.12}$$

Where P_i is intercepted precipitation [cm d^{-1}], P_{gross} is gross precipitation [cm d^{-1}], a is an empirical coefficient [cm d^{-1}] and b is the soil cover fraction [-]. $a \cdot LAI$ is equal to the leaf area saturation. In this formula, leaf area saturation is taken into account. When the leaf area is saturated, no extra water can be intercepted.

2.3.2 Potential evapotranspiration

Potential evapotranspiration is evapotranspiration which is not limited by the amount of available water and by the salinity. So potential evapotranspiration is only influenced by atmospheric circumstances and crop characteristics. Different equations are available to calculate the potential evapotranspiration, such as the Priestley-Taylor equation, the Makkink equation and the Penman-Monteith equation (Priestley & Taylor, 1972; Makkink, 1957; Monteith, 1965). Of all these equations, the Penman-Monteith equation, which is based on the energy balance, is seen as the best equation for all climates (Kroes *et al.*, 2008). One limitation of this equation is that the influence of the CO_2-concentration in the air on the potential evapotranspiration is not taken into account. The Penman-Monteith equation reads:

$$ET_p = \frac{\frac{\Delta_v}{\lambda_w}(R_n - G) + \frac{p_1 \rho_{air} C_{air}}{\lambda_w} \frac{e_{sat} - e_a}{r_{air}}}{\Delta_v + \gamma_{air} \left(1 + \frac{r_{crop}}{r_{air}} \right)} \tag{2.13}$$

In which ET_p is the potential evapotranspiration rate [mm d^{-1}], Δ_v is the slope of the vapour pressure curve [kPa $°C^{-1}$], λ_w is the latent heat of vaporization [J kg^{-1}], R_n is the net radiation flux at the surface of the canopy [J m^{-2} d^{-1}], G is the soil heat flux [J m^{-2} d^{-1}], p_1 is used as unit conversion (=86400), ρ_{air} is the air density [kg m^{-3}], C_{air} is the heat capacity of moist air [J kg^{-1} $°C^{-1}$], e_{sat} is the saturation vapour pressure [kPa], e_a is the actual vapour

pressure [kPa], r_{air} is the aerodynamic resistance [s m^{-1}], γ_{air} is the psychometric constant [kPa $°C^{-1}$] and r_{crop} is the crop resistance [s m^{-1}].

The amount of soil evaporation is often limited due to limited water transport to the upper soil. Two methods can be used for the simulation of soil evaporation with the Penman Monteith method: the Latent Heat Index can be used, or the soil cover fraction can be used. When using the Latent Heat Index, the aerodynamic term in the Penman-Monteith is neglected due to the large aerodynamic resistance caused by the small wind speed near the crop (Ritchie, 1972). Therefore radiation is the only energy source for soil evaporation. The potential soil evaporation reduced by crop shadowing can be explained by (Goudriaan, 1977; Belmans *et al.*, 1983):

$$E_p = E_{p0} \cdot e^{-\kappa_{df} \cdot \kappa_{dir} \cdot LAI} \tag{2.14}$$

Where E_p is the potential soil evaporation [mm d^{-1}], E_{p0} is the potential soil evaporation for a wet, bare soil [mm d^{-1}], κ_{df} is the extinction coefficient for diffuse visible light [-] and κ_{dir} is the extinction coefficient for direct visible light [-]. In here the net radiation is expected to decrease exponentially by the LAI. When the LAI is not available for the different crop development stages, the soil cover fractions are used. Then the potential soil evaporation is calculated by the potential soil evaporation for a wet, bare soil with the fraction of bare soil taken into account (Kroes *et al.*, 2008).

2.3.3 Actual evapotranspiration

The actual evapotranspiration can directly be determined by using Penman-Monteith with higher canopy and air resistances. These resistances are higher than the resistances for a dry crop, because of the water vapour diffusion. For many crops these resistances are not yet known, therefore a two-step approach is mostly used to obtain the actual plant transpiration. In here the first step is the calculation of the potential evapotranspiration with minimum resistances. Thereafter the reduction in root water extraction by drought stress, wet stress or saline stress is calculated (Bouten, 1992). Drought and wet stress can be calculated by macroscopic models or microscopic models. For macroscopic drought and wet stress, the Feddes reduction function is one of the most used reduction functions. In this reduction function, the potential root water exchange is multiplied with a reduction factor (α_{rw}). This reduction factor reduces when facing drought stress or waterlogging stress, as is shown in figure 2.2 (Feddes *et al.*, 1978). The parameters h_1, h_2, h_{3l}, h_{3h} and h_4 are

known for different crop types. A more process-based approach is developed for the simulation of waterlogging stress, combining macroscopic and microscopic oxygen diffusion processes. In this approach, the minimum soil gas filled porosity required for oxygen supply is calculated for different abiotic and biotic factors (Bartholomeus *et al.*, 2008). At drought stress, it is expected that reduced water uptake by roots can be compensated by extra water uptake at other roots in wetter spots. Several approaches are developed to include this compensation, for example by introducing a root adaptability factor (Šimůnek & Hopmans, 2009) or by implementing an implicit compensation mechanism (de Jong van Lier *et al.*, 2008). Although this compensation causes a reduction in drought stress, it is estimated that the overestimating of drought stress by models which do not take this compensation into account is minor (Bartholomeus *et al.*, 2015c). This is due to the redistribution of soil moisture by models already.

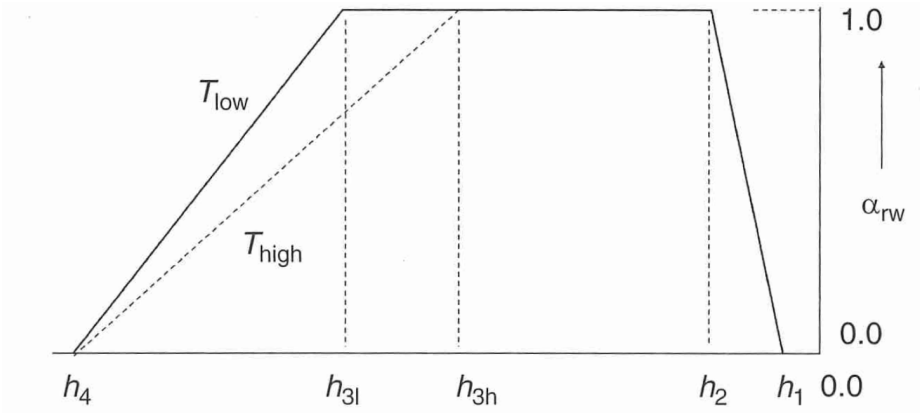

Figure 2.2: The height of the reduction factor (α_{rw}) of the Feddes-function for different critical water pressure heads (h_1, h_2, h_3 and h_4). T_{high} is a high atmospheric demand, T_{low} is a low atmospheric demand (Moene & Van Dam, 2014).

Soil evaporation can be calculated using Darcy's formula. For this formula, the hydraulic conductivity of the top soil should be given. This part of the soil is exposed to extreme conditions such as rain splashing and crust formation. Therefore it is still not clear if the soil hydraulic functions are also valid for the top few cm of the soil. In order to calculate the actual soil evaporation, Black found a reduction function (Black *et al.*, 1969):

$$\sum E_a = \beta_1 t_{dry}^{0.5} \tag{2.15}$$

Where E_a is the actual soil evaporation [cm d^{-1}], β_1 is a soil spe-

cific parameter [cm $d^{-0.5}$] and t_{dry} is the time after the rainfall [d]. Boesten and Stroosnijder proposed another reduction function (Boesten & Stroosnijder, 1986). They used the sum of the potential evaporation as time variable:

$$\sum E_a = \begin{cases} \sum E_p & \text{for } \sum E_p \leq \beta_2^2 \\ \sum \beta_2 \left(E_p^{0.5}\right) & \text{for } \sum E_p > \beta_2^2 \end{cases} \tag{2.16}$$

Where β_2 is a soil parameter [$cm^{0.5}$].

2.4 Controlled drainage

In this section, a review is given on recent research on subirrigation. Both international research and Dutch research are listed below.

2.4.1 Subirrigation

A lot of research is done on subirrigation to compare it with other irrigation methods, such as sprinkler, drip, surface and centre pivot irrigation. Seepage irrigation allows water table control due to changing water level in the supply well, which changes the pressure of the water in the drains, as can be seen in figure2.3 (Dukes *et al.*, 2010; Bartholomeus, 2015). Besides, subirrigation is better for the plant health due to a lower air humidity and a better weed control (Kazumba *et al.*, 2010; Kacimov & Obnosov, 2016). Because there is no visible water front at subirrigation, there is no erosion and no crust formation at the topsoil (Kacimov & Obnosov, 2016). In the dry upper part of the soil, precipitation water can be stored, which enlarges the use of rainfall (Odhiambo & Irmak, 2015). Seepage irrigation leads to less pollution compared to other irrigation methods. The groundwater is less polluted because there is less flow to the groundwater. Besides, the absence of contact between effluent and agricultural activities leads to less pollution of groundwater and surface water (Kazumba *et al.*, 2010). Furthermore, there is a reduction of air pollution by aerosols, caused by the absence of surface irrigation. irrigation is easy to use and brings low infrastructural costs (Dukes *et al.*, 2010). At last, subirrigation is more suitable for fields with an irregular shape than other irrigation methods (Odhiambo & Irmak, 2015).

There are also some disadvantages of subirrigation. It has a lower water use efficiency than other irrigation methods (Reyes-Cabrera et al. 2016). Besides, in heterogenic soils, the fine fraction can move downward due to high hydraulic gradients near the drains (Kacimov

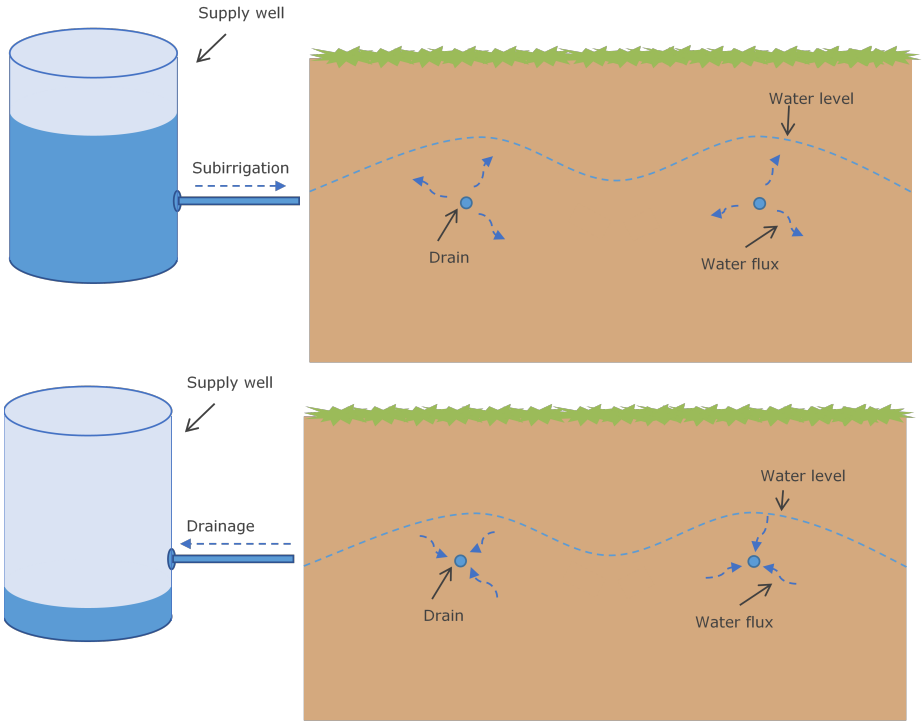

Figure 2.3: The working of subirrigation. When the level of the supply well is higher than the drain level (upper situation), water will flow in the drains and will flow into the soil. The higher the water level in the supply well, the higher the pressure in the drains and the more subirrigation. When the water level is lower than the supply well (lower situation), water will drain from the soil to the supply well.

& Obnosov, 2016). Moreover, although wind has no influence on the uniformity of subirrigation, the soil variability causes a higher variability in moistening than with above ground irrigation (Dukes *et al.*, 2010). At last, at sandy soils water suction is limited and therefore only shallow drains can provide enough water to the roots (Reyes-Cabrera *et al.*, 2016).

2.4.2 Controlled drainage in the Netherlands

The last decade there were several experiments with subirrigation in the Netherlands. In 2008 a model study was done about controlled drainage and composite controlled drainage (van Bakel *et al.*, 2008). At (composite) controlled drainage, some groundwater will be held inside the field by not draining all groundwater. Hereby, surplus water can be temporary stored for dry times, so less irrigation water is needed in dry periods. Water retention can be accomplished by

controlling the water level of the ditch, which determines the amount of irrigation water discharged by drains to the ditch. Controlled drainage is the more simplified way, in which the water level of the ditch will be controlled by a weir. With composite controlled drainage, the drain pipes are not directly connected to the ditch. Instead, they are connected to a collection pipe. The amount of water drained to the ditch is determined by the level of a regulating well, which connects the collection pipe with the ditch. The level of the regulated well can be controlled manually. By (composite) controlled drainage, water retention can reduce the use of irrigation water and increase the crop yield. Besides, (composite) controlled drainage allows high groundwater levels in nature areas and low groundwater levels in arable areas next to each other (Stuyt *et al.*, 2012).

A more complex and detailed way to regulate groundwater levels is climate adaptive drainage. Hereby, sensors and weather forecasts detect water shortage or water excess in an early stage. The predicted water shortage or water excess can be reduced by subirrigation or drainage (Bartholomeus *et al.*, 2015b). Since 2011 research is done on climate adaptive drainage. There has been carried out a model study and multiple experiments with climate adaptive drainage on three locations (Terink *et al.*, 2013). The participated farmers were satisfied. The research shown that climate adaptive drainage is financially viable in most areas. Only in areas with leakage or iron precipitation, climate adaptive irrigation is not financially viable. With leakage no water can be stored and iron precipitation causes the drains to be clogged (Terink *et al.*, 2013).

Currently, next to the experiment with Bavaria water, two other experiments are being conducted in the Netherlands with the reuse of treated wastewater for the agricultural sector. One experiment is done in Haaksbergen and the other in Delft. Waterschap de Vechtstromen test the reuse of sewage water for subirrigation (Bartholomeus *et al.*, 2015a). In Delft a test is going on with the reuse of sewage water for irrigation water in greenhouses. Next to the few implementations in the agriculture, in the Netherlands there are more general implementations with the reuse of industrial wastewater. For example a potato company, a producer of intermediate goods, a sugar producer, a chemical company, a trade organisation and a paper factory are reusing their wastewater (Colsen, 2012; Raap, 2010; Natuurlijk Kapitaal, 2016; Croda, 2014).

Chapter 3

Study area

The Bavaria brewery is located in Lieshout and the test field is in Aarle Rixtel, both in the south of the Netherlands. Figure 3.1 gives an overview of their locations. The study area is part of the land of a farmer, with mainly grass and at a small part maize on it. Analysis of the geographical and geohydrological situation show that the area consists of a landscape of cover sand, with a weak relief (Jalink *et al.*, 2000). The topography of the study area is shown in figure 3.2. The top formation is the Nuenen group, which is a heterogenic group with layers of sand, loam and peat (Jalink *et al.*, 2000). The top five meter of the Nuenen group in the study area is shown in figure 3.3. Due to the less permeable soil layers, local shallow groundwater tables exist. Hereby the irrigation water will not infiltrate to lower layers quickly and the subirrigation can raise the groundwater table. The formation of Sterksel and Veghel is located below the Nuenen group and consists of coarse sand (Schrama & Jalink, 1998). In this formation, a closed layer of the clay of Rosmalen exists with a thickness of two to ten meter (Rijkswaterstaat, 1985). Below the formation of Sterksel and Veghel, the clays of Kedichem and Tegelen form an aquitard and can be seen as the vertical water divide. Below this, the formation of Tegelen consists of course sand and gravel (Jalink *et al.*, 2000). Figure 3.4 gives a simplified overview of the soil formations.

The soil map of the study area shows that the soil consists of anthrosols with sand and loamy sand. The average highest groundwater table is 100 – 120 cm below surface and the average lowest groundwater table is 200 – 240 cm below surface (Stichting voor bodemkartering, 1981). The Goorloop and the Wilhelmina canal are the two surface waters in the surrounding area (see figure 3.1). The water level of the Goorloop varies between 12.5 and 13.6 m +NAP, according to hourly measurements of the water board Aa and Maas.

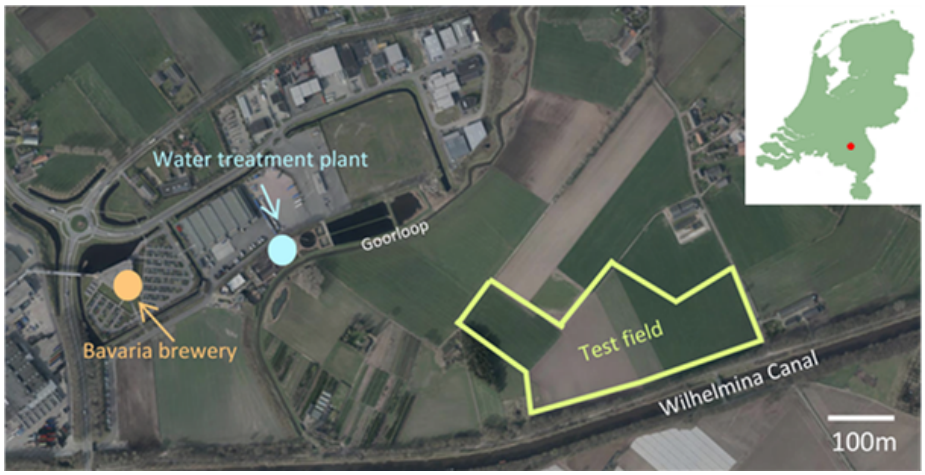

Figure 3.1: The locations of the Bavaria brewery, the water treatment plant, the test field and the two surface waters. From Actueel Hoogtebestand Nederland. The map of the Netherlands in the right shows the place of Aarle Rixtel.

The height difference between the bottom of the Goorloop and the surface level of the study area is approximately 4 m. According to Rijkswaterstaat, the water level of the Wilhelmina canal south of the study area is about 15m +NAP. There is no flow from the Wilhelmina canal to its surroundings (Bartholomeus, 2015). Figure 3.5 shows the water level of the Wilhelmina canal and the Goorloop with respect to the soil surface of the study area.

In the study area, a drainage system has been installed. Figure 3.2 shows the locations of the collection tubes and the supply and outlet wells in the test field. With the use of an adapted formula of Hooghoudt and the model SWAP, the distance between the drains was calculated by KWR to be 10 meter. The currently used collection pipe has a diameter of 160 mm and is located 15.4 m +NAP. The second collection pipe is placed for future drainage outside the study area, but is not used at this moment. The drains are placed at a depth of 15.5 m +NAP in the sandy soil. The depth of the drains below surface differs from less than one meter to over 1.5 meter and all drains are located in soil with a high hydraulic conductivity. The supply well delivers water to the area and has a diameter of three meter. The water level in the supply well determines the water pressure in the drains. In the winter, the water delivery will stop and the drains will then be used to drain the area. Ventilation tubes at the end of the drains ensure air can leave and water can enter the drains. The outlet well will remove the drained water from the area (Bartholomeus, 2015). The subirrigation in the study area started

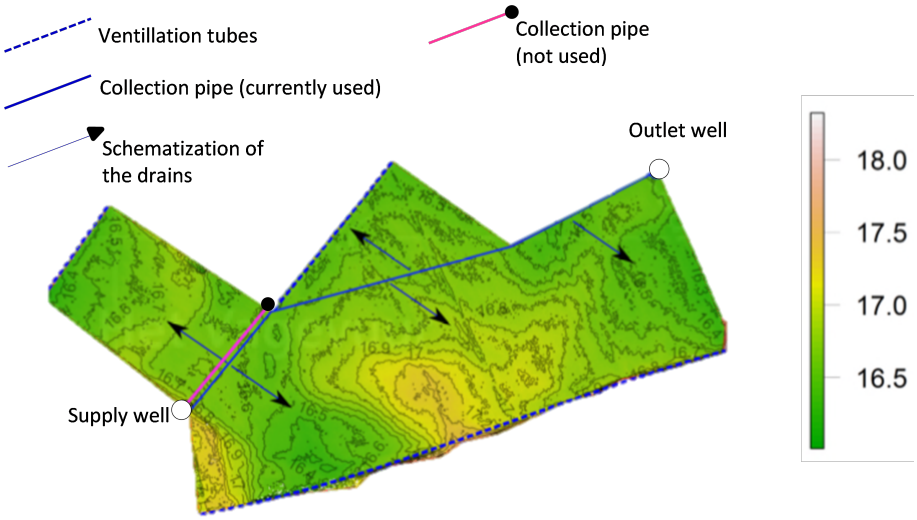

Figure 3.2: The topography of the study area, in height of the surface above NAP. The locations of the supply well, the collection pipe, and the ventilation tubes are also shown. The arrows give an impression of the place and direction of the drains, but the drains itself are not drawn in the figure. (Bartholomeus, 2015).

in 2016. In that year the subirrigation was applied from May till October. The amount of subirrigation is shown in figure 3.6.

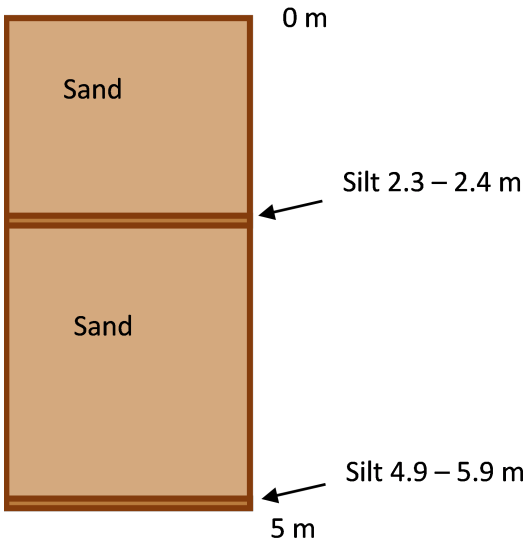

Figure 3.3: An overview of the top five meter of the nuenen group in the study area. All depths are here in meters below surface (Bartholomeus, 2015).

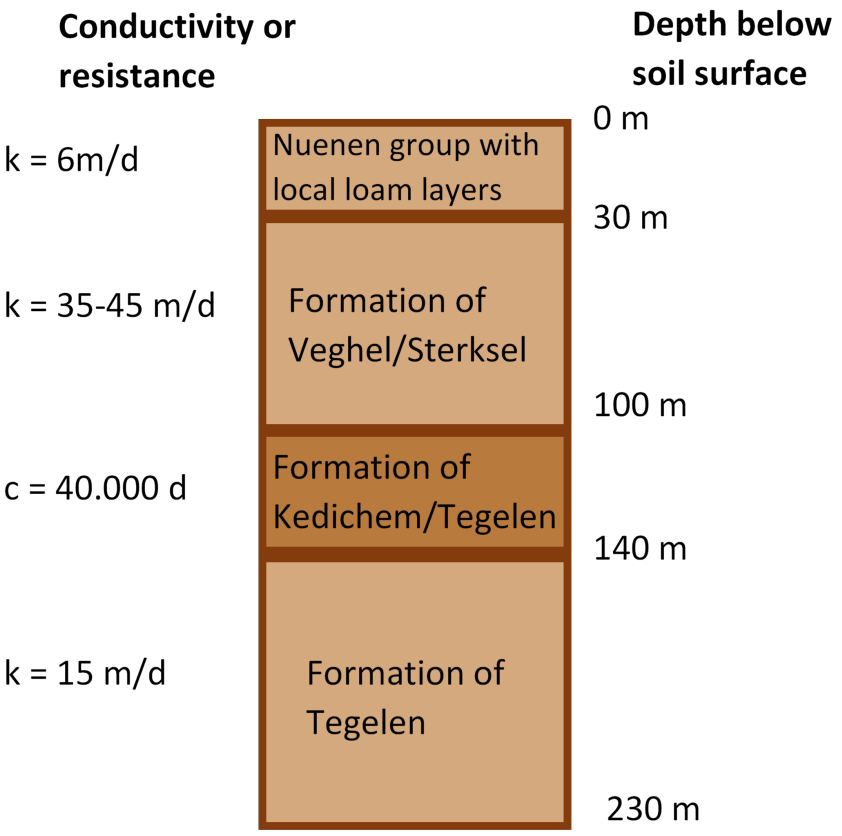

Figure 3.4: A simplified overview of the soil formations in the study area and their conductivity/resistance (Broks, 1989).

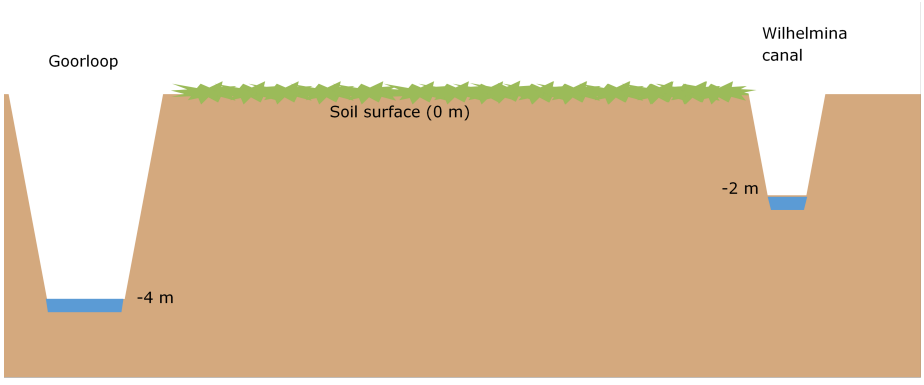

Figure 3.5: The water level of the two rivers near the study area. The levels are with respect to the soil surface.

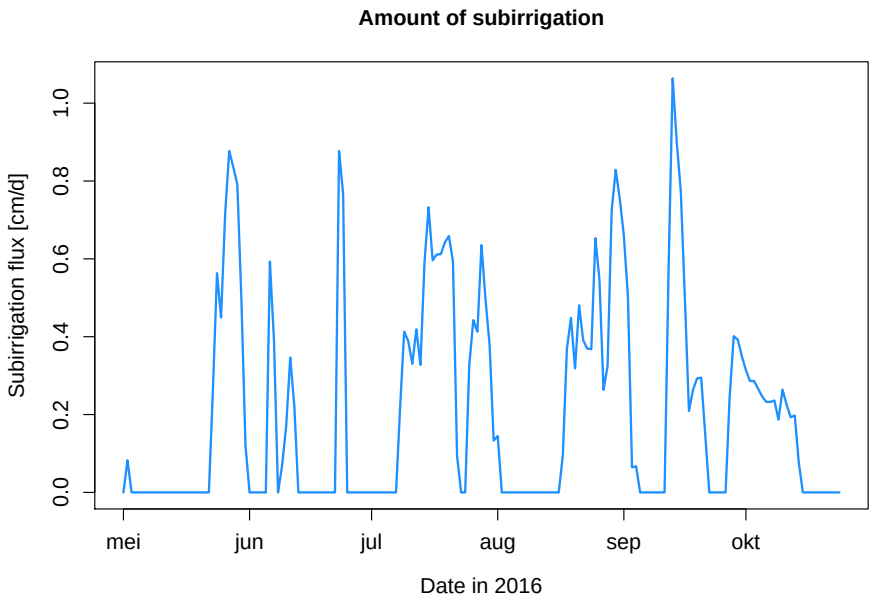

Figure 3.6: The amount of subirrigation applied in the year 2016 the study area.

Chapter 4

Methods

The two research questions as formulated in the introduction chapter are:

- What is the optimal subirrigation water head in the study area to achieve the highest crop yield?
- To which extent does the soil temperature change due to the subirrigation?

The first research question was investigated by using a SWAP-WOFOST model for the study area. Most of the input for the SWAP-WOFOST model came from measurements done by KWR. However, the van Genuchten parameters, which describe the soil hydraulic functions and are input for SWAP, were not yet known. These parameters were investigated through soil samples in the laboratory. Hereby, the evaporation method was used (Wendroth *et al.*, 1993). Eventually, the model was calibrated for the water and heat fluxes in the year 2016. Soil temperature measurements were done and were used in this calibration. After the calibration, for each scenario the drain pressure level was obtained that leads to the highest crop yield. The second research question was as well investigated by the calibrated SWAP-WOFOST model. Besides, this research question was also examined by analysis of the soil temperature measurements.

Figure 4.1 shows the locations of the measurements done by KWR. At point A4 most of the measurements were taken. This is also the spot where the soil sample was taken for the evaporation method and where the temperature sensors were placed. KWR had measured the water level at 2, 5 and 9 m below surface hourly at point A5. At point A4, the soil moisture content at 20, 40 and 60 cm below surface and the groundwater level were measured every

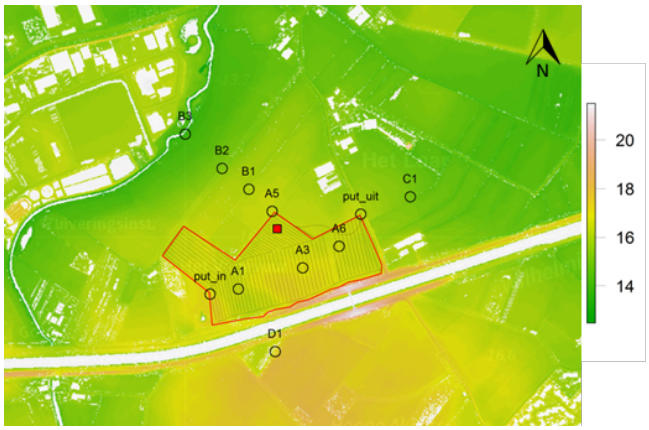

Figure 4.1: The locations of the measurements done by KWR. The red square is point A4. At point A4 also the temperature sensors were placed and soil samples were taken for the evaporation method.

15 minutes. Also the pressure in the drain and the temperature in the drain were measured here, these are hourly measurements. All these measurements were taken from March 2016 till November 2016. At the supply well the water level in the supply well and the water flux from the supply well were measured every five seconds by Bavaria. These measurements are taken from May till October 2016. For SWAP only daily values of the measurements are used.

4.1 Evaporation method

The Van Genuchten parameters were estimated for 20, 40 and 60 cm below surface by the evaporation method. With the evaporation method, a saturated undisturbed soil sample was placed on a balance. The soil sample had four tensiometers in it. While the sample evaporated, the hydraulic head measured by the tensiometers and the weight of the balance were measured every minute. At the end, by using the Wind method simulated fluxes and heads were compared to the measured ones (Wind, 1968; Halbertsma & Veerman, 1994; Boels *et al.*, 1978). By this inverse modelling $\theta(h)$ and $K(\theta)$ relationships were found and were used to obtain the Van Genuchten parameters. It should be noticed that the $\theta(h)$ and $K(\theta)$ relationships are only valid within the measurement range.

4.1.1 Sample collection

Nine undisturbed soil samples were collected. The soil samples were taken at location A4 (see figure 4.1) at three depths and three distances from the drain, as is shown in figure 4.2. The soil samples were collected inside PVC rings. Figure 4.3 shows such a PVC ring. The rings are 8 cm high and have a diameter of 10 cm. Each ring has four holes, each 1 cm in diameter. The holes are placed at a height of 1, 3, 5 and 7 cm from the bottom of the ring. The rings were cleaned and tape is sticked on the inner side of the rings. Through this the holes inside the ring were covered, so soil could not fall out through the holes. The samples were taken by digging a hole at the three locations. First to 15 cm below surface, then to 35 cm and finally to 55 cm below surface. The ring was placed in the hole. On top of the ring a shelf was placed and with a hammer the ring was beaten into the ground. Carefully, the ring was dug out of the soil with a garden trowel. The upper and lower side were prepared with a small saw. The saw was used perpendicular to the sample. By this, the upper and lower side became a smooth plane, without smearing the sample. A cover was placed on the lower side of the sample and the upper side was covered with cling film. This procedure was repeated at other locations and depths for the rest of the soil samples.

Figure 4.2: The locations of the collected soil samples.

In the laboratory the cling film was removed from the samples. With a needle the tape on the inner side of the lowest hole was removed. All samples were placed in a container with a layer of approximately 4 cm of water. The cover on the lower side of the sample and the PVC ring were not connected seamlessly, so water from the container flowed through these openings and through the lowest hole to the sample. The soil samples were left for a few days in the container, until they were fully saturated with water.

Figure 4.3: The PVC rings in which the soil samples were kept for the evaporation method.

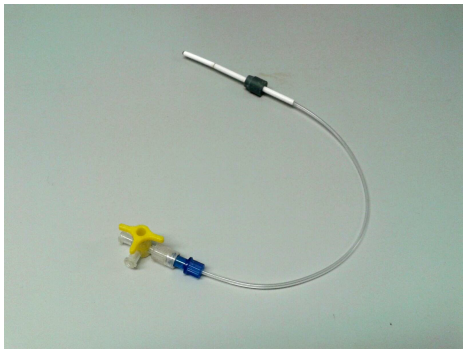

Figure 4.4: A conventional tensiometer which was used in the evaporation method. The yellow tap can be turned and only tubes which are in the direction of the yellow pointers are connected.

4.1.2 Sample installation and measurements

The computer program Lantronix was used to monitor the soil water pressure heads and balance weights. The samples and tensiometers were turned on in the program and specifications were inserted for the samples, such as sample name and length of the tensiometer. At the calibration the tensiometers were still standing in a measuring cup with water. The water level inside the measuring cup was set at the same height as the middle of the lowest pressure transducer. By the computer program, the tensiometers from the lowest to the highest pressure transducer were calibrated at 0, 2, 4 and 6 cm respectively. The calibration values were saved an noted.

Before the samples could be installed, the tensiometers and pres-

sure transducers were de-aerated. In appendix A the procedure used by the de-aeration is explained. During the installation of the samples, a cover was placed on top of all samples. Cellophane was used to make the connection between the bottom cover and the soil samples. A hole was made inside the cellophane so the lowest hole in the PVC ring was still reachable. A hole was made in the tape on the inside of all holes in the PVC ring. A dummy tensiometer without ceramic cup was placed in one of the holes. Through this dummy, a drill with a diameter of 2 mm was inserted. By this a horizontal hole was pre-drilled for the tensiometer, so the tensiometer encounters less resistance when pushing inside the sample. Then the tensiometer was carefully pressed inside the sample hole at the same height as its pressure transducer. This was also done with the other tensiometers. The sample was dried at the underside and was placed on the balance. The tubes were placed on a tripod in such way that they were hanging free and were not in contact with the balance. When all samples were installed, the covers on top of the samples were removed. The final installation of a soil sample was shown in figure 4.5. From now on the measurements were started. Every minute the hydraulic head of all tensiometers and the weight of the balance were saved. Three times a week the head and weight development were checked. If the underpressure inside the sample becomes high, the tensiometer can give failures. Then the tensiometer becomes permeable under dry conditions. A sample was finished when one of the tensiometers measured a head of about -500 cm and at least two tensiometers did not show failures.

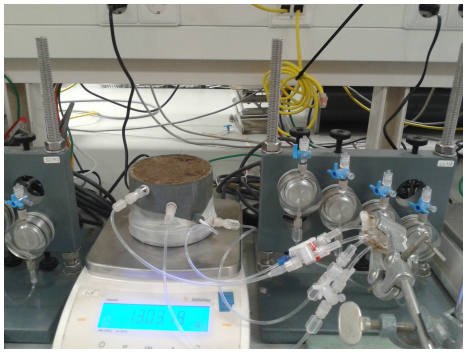

Figure 4.5: The installation of a soil sample. Tensiometers inside the soil sample were connected with pressure transducers.

When the measurements of a sample were finished, the sample was taken out of the ring and put into a metallic bowl. The weight of the sample with metallic bowl was noted down and the sample

was stored in an oven at 105 °C for two days. After the two days, the sample was put out of the oven and was cooled down for half an hour. Then the sample with the bowl was weighted again.

4.1.3 Data analysis

Analysis software made by G Bakker and M Heinen (Bakker *et al.*, 2015) was used to analyse the data. The first step in the analysis was the filtering of the data of each sample. For this step, the excel file *E.Filter V6.4* was used. In here the mean volumetric water content per time step was added to the data, which was calculated from the measured sample weight. The date filter also sorted the measurements to three categories:

- Measurements which could be used for both $\theta(h)$ and $K(\theta)$ determination;
- Measurements which could only be used for the $\theta(h)$ determination;
- Measurements which could not be used later on.

A more detailed description of the filtering of the data can be found in appendix B.

After the filtering and sorting of the data, the data was fitted by using the excel file *E.Fit V3* and Wind Prefit software (Bakker *et al.*, 2015). In the prefit, the parameters of the following van Genuchten relationship were estimated:

$$\frac{\theta(h) - \theta_{res}}{\theta_{sat} - \theta_{res}} = \sum_{i=1}^{k} \omega_i (1 + (\alpha_i h)^{n_i})^{-m_i} \tag{4.1}$$

Where k is the number of modality [-], ω is the weighting factor for multi-modality [-] and i is a counter [-]. The parameters were estimated in such way that the sum of the water content at the four compartments and the total water content calculated had the least differences in sum of squares. Different options could be chosen for the estimation of the parameters. The modality k could be specified as 1, 2 or 3. Besides, instead of using the sample weight, the mean water content could also be used. At last a choice could be made to use the starting water content or the final water content as fixing point. The best options were chosen by trial and error. In the end of this paragraph the estimation of the best options is explained.

After the estimation of the parameters, the hydraulic conductivity was calculated by Darcy's formula:

$$K = -\frac{q}{\frac{dh}{dz} - 1} \tag{4.2}$$

The conductivity was calculated by assuming four horizontal compartments in the soil sample, with a tensiometer halfway the compartment. Compartment 1 is the most upper compartment and compartment 4 is the lowest compartment. The difference in the estimated water content in compartment 4 between two time steps can be interpreted as the water flux between layer 4 and layer 3. The water flux between layer 3 and 2 can be calculated by the difference in estimated water content of layer 3 between two time steps, taken into account the flux between layer 4 and layer 3. The water flux between the other layers can be calculated in a same way. In that way three water fluxes at the intersections of the compartments were calculated. $\frac{dh}{dz}$ was calculated at the intersections by the difference in head averaged over the two time steps and by the height of the compartments. Because of the upward flux, the $\frac{dh}{dz}$ values can only be higher than 1 in order to have a positive K. Now the head and the volumetric water content could be determined at the intersections of the compartments, either by arithmetic averaging or by geometric averaging. The determined θ, h and K at the intersections for every time step were used to calculate the unimodal Van Genuchten parameters. In here the RETC software (Leij *et al.*, 1992) was used. The *E.Fit V3* excel file showed also graphs of the pF curve, the $K(h)$ curve and the $w(t)$ curve. An example of the pF curve is shown in figure 4.6. In these curves, the data points, the pre-fit curve and the curve of the final fit are displayed.

For all variations in ending points and tensiometers included per sample, as obtained by the data filtering, the data was fitted by *E.Fit V3*. At first all variations were fitted by using the default values. In here, the modality, which is a parameter of the shape of the soil water retention curve, was set to 2 and the sample weights were used for the prefit. Also the starting water content was used as fixing point in the prefit and the arithmetic mean was used for averaging the θ and h values. Then for every data, one of the parameters was changed, by keeping the other three parameters at default values. This was done for all parameters. The graphs of all parameter options and variations in ending points and tensiometers included per sample were compared. It was checked if the measurement points in the $K(h)$ graph range over a high variation in hydraulic head. Besides, care was taken if the fitted pF curve and the fitted $w(t)$ curve

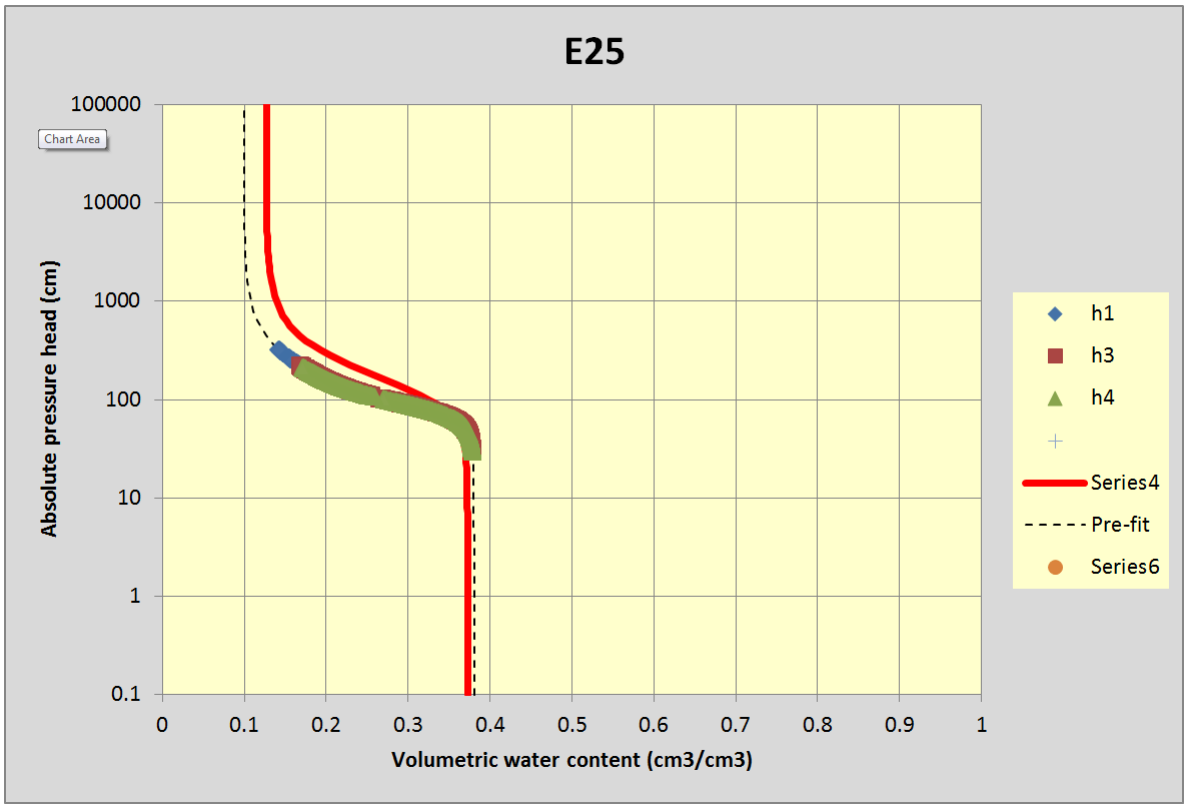

Figure 4.6: An example of one of the output graphs of the excel Fit file. In here the blue, red and brown dots are measurements. The dotted line is the prefit and the red line is the final fit.

corresponds to the measurements. The van Genuchten parameters of the best fit per sample were taken. Now these parameters were averaged for the samples which were taken at the same depth. By this, the van Genuchten parameters at a depth of 20, 40 and 60 cm below surface were obtained.

4.2 Temperature measurements

Continuous temperature measurements were taken to investigate the influence of the irrigation water temperature on the temperature of the soil. These measurements were taken at 20, 40 and 60 cm below surface and on a horizontal distance of 0, 200 and 380 cm from the drain.

The temperature sensors used were the Campbell Scientific Model 107 Temperature Probes with a cable length of three meters. These

sensors have a maximum error of ±0.2°C over 0°C to 50°C (Campbell Scientific, 1983). Ten sensors were calibrated in a temperature controlled water container in a room with a constant temperature and humidity. The sensors in the container are connected to a computer and with the program PC200W of Campbell Scientific. The measurements were stored with a frequency of once a minute. The water in the container was first set on a temperature of 25°C. Next the temperature was decreased to 20, 15, 10 and 5°C. Thereafter the temperature was increased again to 10, 15, 20 and 25°C. The decrease and increase in temperature were both necessary to obtain the deviation in the measured temperature for both increasing and decreasing temperatures. It was assumed that the temperature of the water was constant half an hour after changing the temperature. After this half an hour, the temperature was kept constant for an hour. Per sensor the mean deviation between the measured temperature and the temperature of the water was taken as the calibration value. This value was used later on in the calculations of the temperature measurements.

The nine temperature sensors with the smallest calibration value were installed in the field at location A4 (see figure 4.1). The sensors were installed at 20, 40 and 60 cm below surface at a distance of 0, 2 and 4 m from the drain, as is shown in figure 4.7. The sensors were connected to a Campbell Scientific R1000 data logger. The data logger was connected to a battery and the data logger and battery were placed inside a locker. The locker was fixedly put into the ground with a pole. The installed locker with the battery and data logger is shown in figure 4.8. The temperature sensors were installed by sticking them horizontally in the soil. Then the datalogger was connected with a computer and with the computer program PC200W the measurements were started. Every minute the measured temperature from the nine sensors was saved in the data logger.

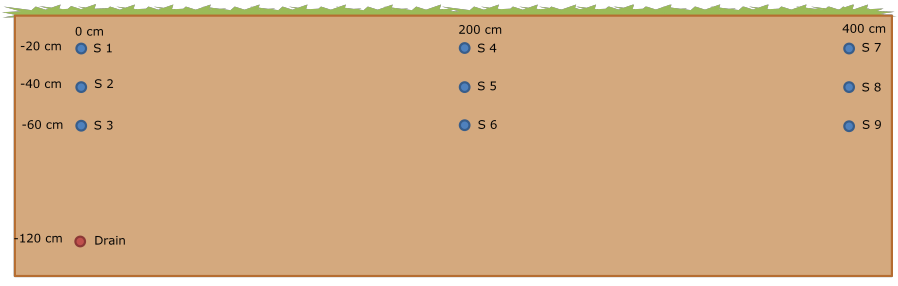

Figure 4.7: The locations of the installed temperature sensors.

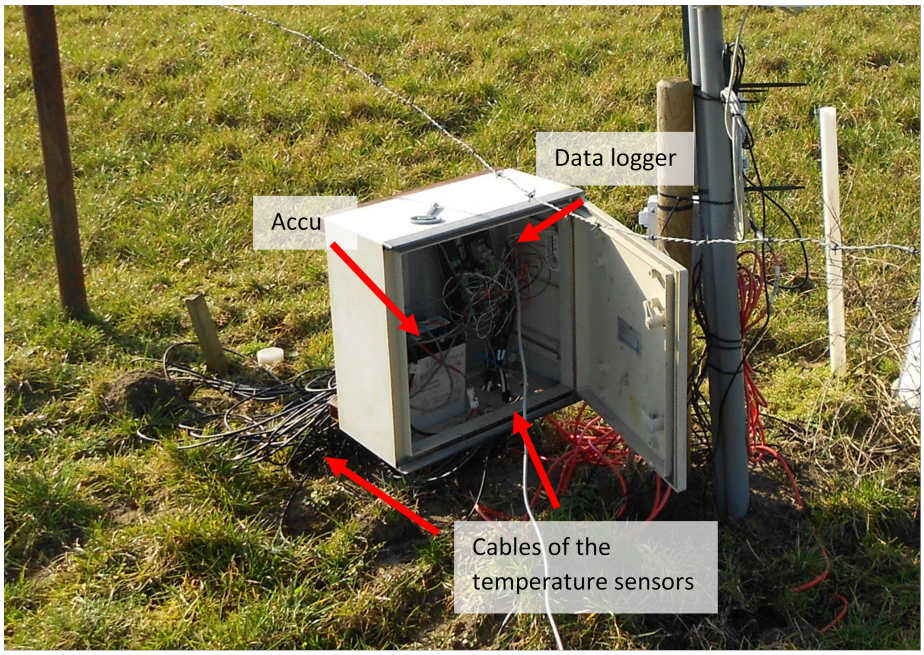

Figure 4.8: The installed locker with the datalogger and accu in it. The datalogger is connected with the temperature sensors.

Three times, a laptop with the program PC200W was connected to the data logger and the measurement data was copied to the computer. For the data elaboration first for every depth the three measurement series were compared to each other. Thereafter a linear regression was made to compare measurements of the same depth next to the drain and two meters from the drain. Also with linear regression measurements of the same depth next to the drain and 4 meter from the drain were compared. The linear regressions were done with a 90% confidence interval. Also the variation in the temperature (dT/dt) of the three measurements at the same depth was compared to each other. Further on, a multiple linear regression was taken. The dependent variable was $T_{next\,to\,drain} - T_{4m\,from\,drain}$ or $T_{next\,to\,drain} - T_{2m\,from\,drain}$. This was done for all depths separately. All dependent variables were used once every hour. The independent variables of the multiple linear regression were the drain pressure (corrected for the changes in air pressure), the drainage temperature, the sub-irrigation flux, the air temperature and the global radiation. The global radiation has not a Gaussian distribution, because a radiation of zero occurs relatively often. Therefore the global radiation itself cannot be used as input for multiple linear regression. That is why it was chosen to use a discrete time series of

hours, where hours without radiation got a value of 0 and hours with radiation got a value of 1. The hourly data of the drain pressure, drain temperature and sub-irrigation flux came from measurements of KWR. The hourly measurements of air temperature and global radiation came from the KNMI, weather station Eindhoven. With the use of ANOVA it was investigated if the relation became better by adding a variable. Eventually the best multiple linear regression per dependent variable was plotted in a plot with also the dependent variable, to see if the regression can simulate the variable correctly.

4.3 SWAP-WOFOST model

SWAP is a deterministic model which simulates the interaction between vegetation and the transport of water, heat and solutes in the unsaturated zone. The model focuses on the field scale. Figure 4.9 gives an overview of the transport processes in SWAP. The top of the model is just above the canopy and the shallow groundwater marks the bottom of the model. The model is one dimensional, because the transport processes in the unsaturated zone are mainly vertical. The model requires general input on for example soil water and heat flow. Next to this general input, meteorological input of the simulated years is required. Optional are the crop growth input and the drainage data (Kroes et al. 2008).

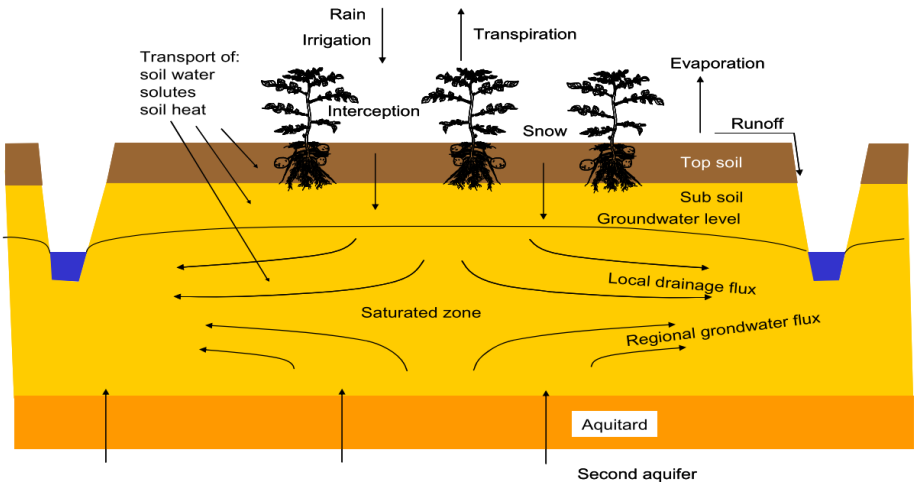

Figure 4.9: The main processes taken into account in the SWAP model (Kroes *et al.*, 2008).

SWAP uses a modification of the Mualem-van Genuchten function and the Richards equation to simulate water flow. When the

rain intensity is too high or the groundwater table is too high, it also simulates ponding and runoff. SWAP considers soil evaporation, transpiration and interception separately. The actual plant transpiration is calculated by the two-step approach. First the potential transpiration is calculated. After that, reduction function(s) as explained in paragraph 2.3.3 are applied (Kroes *et al.*, 2008).

The detailed WOFOST-module is linked with SWAP to calculate the growth rate of the different parts of the crop. Figure 4.10 shows the main processes taken into account by WOFOST. The amount of assimilates is calculated by the light absorbed by the crop and the amount of water stress. The increase in dry matter is calculated by substracting the maintainance respiration and the growth respiration from the assimilates. Senescence is calculated separately for stems, roots and leaves. The amount of senescence of the stems and the roots is only dependent of the development stage. For the senescence of the leaves also water-stress, shading and exceedance of the lifespan is taken into account. Eventually the net growth is calculated (Kroes *et al.*, 2008).

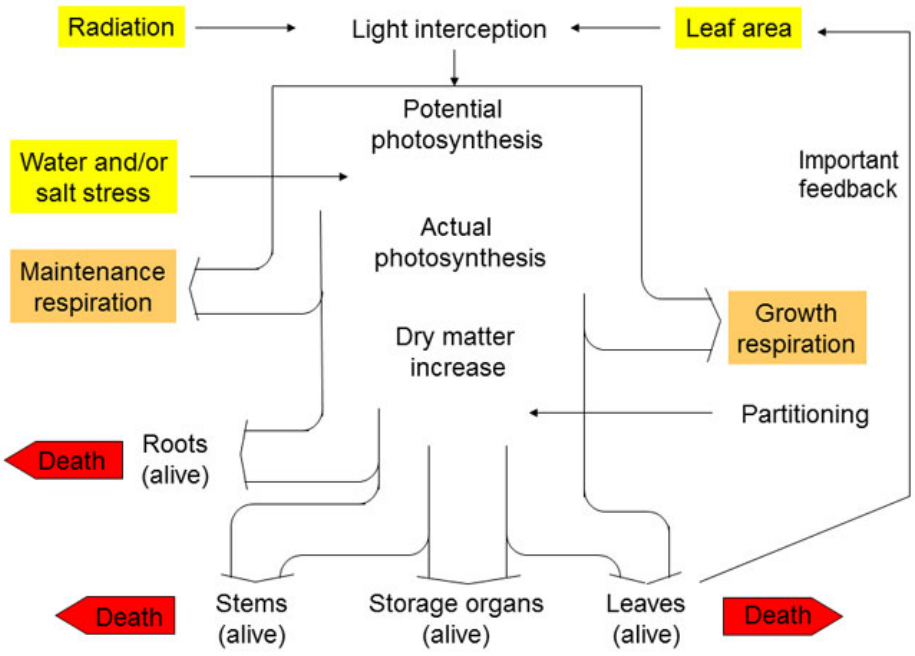

Figure 4.10: An overview of all processes taken into account in the WOFOST model (Kroes *et al.*, 2008).

4.3.1 Implementing extra heat flux in SWAP

SWAP originally only simulates vertical heat flow, with the atmospheric conditions as heat source. To simulate the heat flow coming from the irrigation water properly, an extra heat source had to be implemented. This extra heat source was implemented in the differential equation for soil heat flow, only at the node where the drain exists. The vertical heat flow already implemented in SWAP is responsible for a redistribution of this extra heat within the soil. Without extra heat source, the differential equation reads:

$$C\frac{\partial T}{\partial t} = \frac{\partial\left(\lambda\frac{\partial T}{\partial z}\right)}{\partial z} \tag{4.3}$$

Where T is the temperature [°C], t is time [d], λ is the thermal conductivity [J cm^{-1} °C^{-1} d^{-1}] and z is the depth [cm]. With the extra heat flux the equation changes to:

$$C\frac{\partial T}{\partial t} = \frac{\partial\left(\lambda\frac{\partial T}{\partial z}\right)}{\partial z} + S_{heat} \tag{4.4}$$

Where S_{heat} is the extra heat source [J cm^{-3} d^{-1}]. This extra heat source is dependent on the subirrigation flux, on the temperature difference between the soil temperature and the irrigation temperature and on the heat capacity. The extra heat source will be higher with a higher subirrigation flux and a higher temperature difference between soil temperature and irrigation temperature. A higher heat capacity will also give a higher heat source. Using these correlations and applying dimensional analysis, the following definition of Sheat could be given:

$$S_{heat} = q_{inf}\left(T_{inf} - Ti\right)C\frac{1}{\Delta z} \tag{4.5}$$

$$q_{inf} = \frac{\phi_{drain} - \phi_{avg}}{\gamma_{inf}} \tag{4.6}$$

In here q_{inf} is the flux of sub-irrigation [cm d^{-1}], T_{inf} is the temperature of the irrigation water [°C], T_i is the temperature of the soil at node i [°C], Δz is the height of node i [cm], ϕ_{avg} is the average groundwater level midway between the drains [cm], ϕ_{drain} is the water level inside de drain [cm] and γ_{inf} is the irrigation resistance of the sub-irrigation system [d].

To calculate heat flow, SWAP uses a finite difference form of the differential equation for soil heat flow, which is written in a tri-diagonal matrix. Appendix C shows how the extra heat source was implemented in this tri-diagonal matrix.

4.3.2 SWAP input

The SWAP input files contain a lot of information. The input was chosen in such a way that the study area was best represented. The simulation interval was set to once a day. The daily meteorological data came from the nearest KNMI measurement station, which is Eindhoven. Three soil layers were assumed, the first layer at 0-30 cm below surface, the second layer at 30-50 cm and the third layer at 50-500 cm below surface, as shown in figure 4.11. These layers were chosen so each layer could be represented by the temperature measurements and by the soil samples used at the evaporation method. The soil texture of these layers came from field observations from KWR. The discretisation of the upper 10 cm was set to nodes of each 1 cm height. Further downward, the nodes became 5 cm and eventually 10 cm thick.

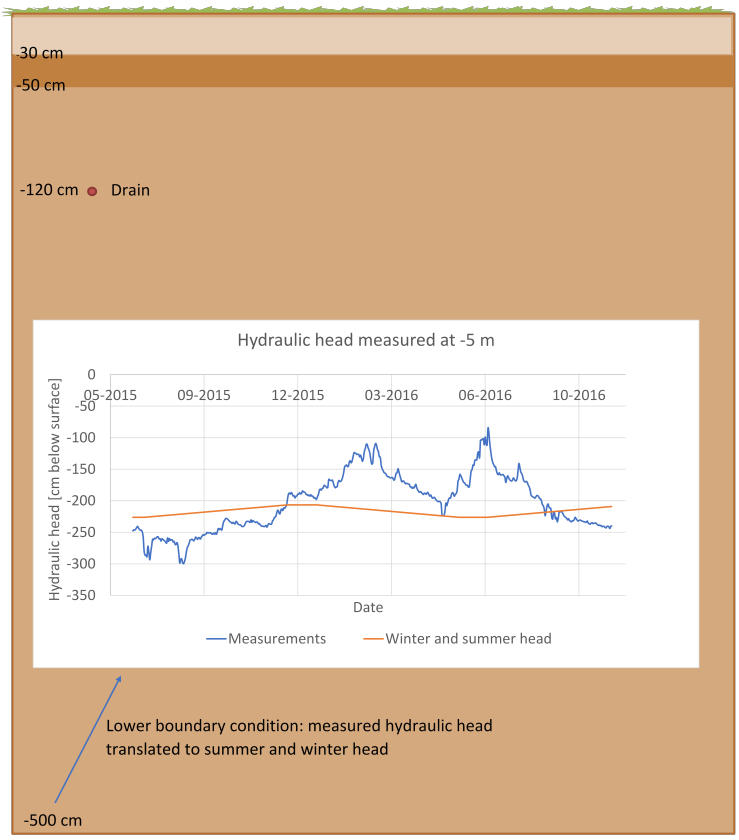

Figure 4.11: An overview of the different soil layers used in the SWAP model. At the lower boundary of the model, at -5 m, the measured hydraulic head, converted to a summer and winter head, is used as bottom boundary condition. The measured and converted head are shown in the graph in this figure.

The moisture conditions were described by initial and boundary conditions. All simulations were already started one year in advance to determine the initial soil moisture. The top boundary was the meteorological input in the model and at the bottom, a Dirichlet boundary condition was used. Here the soil water pressure head at 5 meter below surface was used. KWR had measured this pressure head in 2015 and 2016. The year 2016 was a wet year and in part of this year subirrigation was used, which causes higher heads in 2016 than in 2015. This makes the measurements from 2016 not representative for the current climate. Therefore, although only one year of measurements is somewhat small, only the measurements of 2015 were used. The 2015 pressure heads were used to estimate a summer and a winter pressure head at 5 m below surface. These pressure heads were used as input for the Dirichlet boundary condition. An overview of this lower boundary condition is given in figure 4.11.

The drainage was described as multi-level drainage with fixed resistances. The first drainage level is the Goorloop and the second drainage level are the drains which were used for sub-irrigation. The water level in the Goorloop was described by hourly measurements of 2003 till 2016, measured by water board Aa en Maas. From these measurements, a summer and a winter water level were estimated and these levels are used as input for SWAP. For the drains (the second drainage level), SWAP needs the pressure head inside the drains as input. Only from May 2016 till October 2016 there was subirrigation and therefore only for 2016 measurements could be used as input. These measurements of the pressure head inside the drains were input for the calibration, because for the calibration only the year 2016 was simulated by SWAP. For the investigation of the optimal irrigation pressure heads, the average winter and summer heads were used in stead of the measurements. In here the used pressure heads varied between 30, 60, 90 and 120 cm below surface. For the investigation of the soil temperature, the optimal irrigation heads for grass were used as input.

The drain spacing of the Goorloop was set to 425 meter, which is the distance from the Goorloop to location A4 in figure 4.1. In SWAP all depth levels were assumed to be relative to a reference level, which was taken as the mean surface level of the test field. The depth of the Goorloop was assumed to be 4 m, relative to this reference level. The subirrigation drains have a drain spacing of 10 m and their depth is at 120 cm below surface. For both the Goorloop

and the drains, the waterflux is described by:

$$q_{inf} = \frac{\phi_{drain} - \phi_{avg}}{\gamma_{inf}} \tag{4.7}$$

The detailed grass module was used as input for WOFOST, where grazing is chosen as management input. For waterlogging stress, the reduction by Feddes or by Bartholomeus *et al.* (2008) can be used. The reduction by Bartholomeus *et al.* (2008) was chosen, because of the more process-based simulation of waterlogging stress. For the simulation of drought stress, the Feddes reduction function or the reduction function by de Jong van Lier *et al.* (2008) can be used. Here was chosen for the Feddes function, because many parameters which were needed for de Jong van Lier *et al.* (2008) are not known for the study area.

For the scenario with climate change, adapted meteorological data were used. These data came from the transformation program of the KNMI, version 3.2 (Bakker & Bessembinder, 2012). Here the KNMI 2000-2010 data of station Eindhoven was used as input. The output was gained for the year 2050, for the four different KNMI climate scenarios. These scenarios are Gh, Gl, Wh and Wl. The scenarios Gh and Gl have a temperature increase of 1 °C between the climate of 1990 and 2050, whereas Wh and Wl have a temperature increase of 2 °C between those two climates. The air circulation pattern will change significantly for the Gh and Wh scenarios, while this pattern will not change much for the scenarios Gl and Wl. It is expected that the increase in winter precipitation would cause a higher winter head at 5 m below surface. However, it is unknown how large the increase in Goorloop level and the increase in head would be. Therefore these effects were not taken into account. Another expected effect of climate change is an increased CO_2 level in the atmosphere. Also this effect was not taken into account, because in WOFOST the CO_2 level cannot be changed yet. For the simulations with potatoes and maize detailed maize and potatoes crop files were used as input for WOFOST.

4.3.3 Calibration

The purpose of the calibration of the SWAP model is to get a model which approaches the measured groundwater levels, soil moisture conditions and soil temperatures. The model was calibrated for the year 2016, i.e. the year with subirrigation. The simulation already started at 2015 to have the right initial conditions at the beginning of 2016. For the calibration, the real measurements were used for both

the head at 5 m below surface and the water level in the Goorloop. So here not only one winter and summer level were used. Calibration was done by eye and by looking at the root mean squared error.

Firstly, the simulated soil moisture contents and water levels were calibrated. Hereby the simulated soil moisture content at 20, 40 and 60 cm depth was compared to measurements at that depths, which came from KWR. SWAP uses heads and no soil moisture contents in its calculations. In the end the heads are transformed in SWAP to soil moisture contents, by using the soil water retention function. So by changing the van Genuchten parameters θ_{res}, θ_{sat}, α and n, the soil moisture calculated by SWAP from the simulated heads changed. Therefore the van Genuchten parameters were changed until the simulations correspond to the measurements. To make the calibration easier, the simulated heads by SWAP were plotted against the measured moisture contents. In this graph also a soil water retention curve was plotted. First the van Genuchten parameters θ_{res}, θ_{sat}, α and n of the pF curve were changed in such way that the measurements match with the pF curve. Then the chosen van Genuchten parameters were used to see if the simulated moisture content matches with the measurements.

Hereafter the simulated groundwater level was compared with measurements of the groundwater level by KWR. By changing the drainage and irrigation resistances of both the Goorloop and the drains, the simulation should correspond with the measurements. In the calibration of the soil moisture content and the water levels, the simulated subirrigation flux and the measured subirrigation flux should have the same value.

Finally, the heat flow was calibrated. The temperature measurements at 20, 40 and 60 cm depth and the simulated temperature were compared to each other. The initial soil temperature and the temperature of the irrigation water were changed to make the measurements and simulations as much equal as possible.

4.3.4 Scenario analysis

The SWAP input files for the different scenarios were used for the analysis. Every scenario was done for the years 2007-2016, with the year 2006 as start-up year. For the climate change scenario, eleven years of transformed data to 2050 were used. In every scenario the head in the supply well was determined where the total crop yield is the highest. The total crop yield is in here the sum of the cumulative dry matter of the crop and the cumulative amount of grazing dry matter. The optimal head was determined every two months.

Table 4.1: An example of the trials of head combinations for one of the climate scenarios to come to the optimal irrigation head. Every trial is a new starting point as is shown in figure 4.12. The first trial is the optimal head for another climate scenario. In this example, after four trials the optimal irrigation head is approached. In here all heads are in cm below surface.

Months	Head trial 1 [cm]	Head trial 2 [cm]	Head trial 3 [cm]	Head trial 4 [cm]
Jan-Feb	-90	-120	-120	-120
Mar-Apr	-90	-90	-90	-90
May-Jun	-60	-60	-60	-60
Jul-Aug	-60	-60	-30	-60
Sep-Oct	-60	-90	-120	-120
Nov-Dec	-90	-60	-90	-90

So January and February had the same irrigation head, March and April had the same head, etcetera. Every year had the same irrigation head. To make the determination of the optimal head less time consuming, only four possible irrigation heads were used. These heads are 30, 60, 90 and 120 cm below surface, which represents a high, average and low irrigation head and no subirrigation.

Figure 4.12 shows an overview of the determination of the optimal irrigation head. First, the optimal irrigation head was determined for the scenario of grass (2006-2016). At first all heads were set to 120 cm below surface, which was the starting point. For this starting point the total crop yield was determined by using the SWAP-WOFOST model. Then every time one irrigation head (of two months) was increased, while keeping the irrigation head for the rest of the months 120 cm below surface. The irrigation heads with the highest crop yield of all simulations was used as starting point for the next simulations. Now every time one hydraulic head was both increased and decreased, while keeping the head of the other months the same as this new starting point. This procedure was continued until the crop yield did not became higher anymore. Now the optimal irrigation heads for the current situation were known. Then the whole procedure to find the optimal irrigation head was repeated for the other scenarios. Now the optimal heads already obtained for another scenario were used as first starting point. Table 4.1 shows an example of the four starting points used to obtain the optimal irrigation heads.

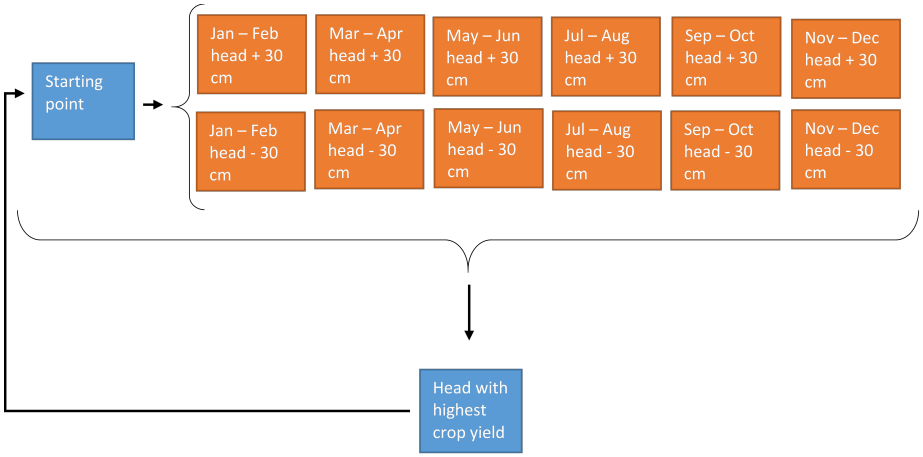

Figure 4.12: The process of determining the optimal irrigation head for every scenario. Simulations were done from the starting point, by every time changing the head of only two months. Of all these simulations the one which gave the highest crop yield was used as next starting point. So in this figure, the yield of all orange boxes were compared to each other and to the yield of the starting point. The situation with the highest yield becomes the new starting point.

Chapter 5

Results

5.1 Evaporation method

Unfortunately, two soil samples could not be analysed by the Wind method. For sample M7, the data filter selects less than 30 measurements which can be used for obtaining the $K(\theta)$ relationship. As at least 30 measurements are needed, this sample could not be analysed. Also sample M9 could not be analysed. This sample had too many variations in the measured sample weight and heads. As the filtering program only selects weights and heads lower than all measured before, not enough measurements were selected for the rest of the analysis. Although sample M3 could be analysed, the outcome of this analysis is not reliable and this sample is therefore also not taken into account. The low reliability is because only measurements with approximately the same measured head were maintained by the filtering of the measurements.

In table 5.1 the van Genuchten parameters obtained by the rest of the samples are shown. In this table, the large differences between the parameters λ and K_{sat} are remarkable, especially at 40 cm depth. There is also a large difference in θ_{res} between different samples, but this parameter is less important for this research, as the residual water content will not be reached in the study area. The other parameters (θ_{sat}, α, n and m) vary only minor between samples at the same depth. The variations in α are so small that all obtained α's are the same when they are rounded.

Table 5.2 shows the van Genuchten parameters for every soil layer. In this table the parameters for the samples at the same depths are averaged. The parameters as shown in table 5.2 are not used directly as input for the SWAP model, because they are first calibrated.

Table 5.1: The van Genuchten parameters obtained for the different soil samples. These parameters are obtained by the evaporation method in combination with the Wind procedure.

Depth sample	Sample name	θ_{res}	θ_{sat}	α	n	m	λ	K_{sat}
[cm]		[cm^3/cm^3]	[cm^3/cm^3]	[1/cm]	[-]	[-]	[-]	[cm/d]
15-25	M1	0.11	0.39	0.01	3.04	0.67	0.00	2.85
	M4	0.14	0.38	0.01	2.68	0.63	-1.27	2.49
35-45	M2	0.00	0.33	0.01	2.57	0.61	-21.26	0.37
	M5	0.22	0.42	0.01	3.35	0.70	0.00	38.68
	M8	0.17	0.41	0.01	3.16	0.68	0.00	5.23
55-65	M6	0.00	0.26	0.01	3.19	0.69	-1.16	4.40

Table 5.2: The van Genuchten parameters obtained by the evaporation method are averaged for every depth.

Depth sample	θ_{res}	θ_{sat}	α	n	m	λ	K_{sat}
[cm]	[cm^3/cm^3]	[cm^3/cm^3]	[1/cm]	[-]	[-]	[-]	[cm/d]
15-25	0.12	0.39	0.01	2.86	0.65	-0.64	2.67
35-45	0.13	0.39	0.01	3.02	0.67	-7.09	14.76
55-65	0.00	0.26	0.01	3.19	0.69	-1.16	4.40

5.2 Calibration

At first, the soil moisture contents and the groundwater levels were calibrated. This was done by changing the van Genuchten parameters, resistance to the ditch and the resistance to the drains. When the soil moisture content and the groundwater levels were calibrated, the simulated irrigation flux was 304 cm/yr, which is nine times as high as the measured irrigation flux of 33 cm/yr (see figure 3.6). It was impossible to get the simulated irrigation flux in the same order as the measured one, while it is important to simulate the irrigation flux correctly. Therefore it was decided to increase the measured hydraulic heads at 5 m below surface, which is input for the lower boundary condition of SWAP. In the calibration, not the calculated summer and winter heads are used, but the measurements of the head itself are used as input. Eventually it was possible to have the simulated irrigation flux at 36 cm/yr, which corresponds to the measured flux. Herefore the measured hydraulic heads were increased with 120 cm, the resistance to the ditch was 8000 days and the resistance to the drains was 80 days. Figure 5.1 shows the measured groundwater level, the measured hydraulic head and the hydraulic head plus 120 cm. It appears that the increased head corresponds in the period with subirrigation fairly to the measurements of the groundwater level.

Figure 5.2 shows the precipitation and the amount of evapotranspiration in the year 2016. Figure 5.3 shows the measured groundwater level, the measured waterlevel in the collecting well and the measured water level in the ditch (the Goorloop). Besides, this figure shows a simulated groundwater level if the groundwater was only affecting by the precipitation and the evapotranspiration. In periods with subirrigation, the measured groundwater level fluctuates more than the simulated groundwater level. This fluctuation has the same pattern as the fluctuation in water level of the supply well. The water level in the ditch corresponds much less to the variation in the groundwater level. This explains why the calibrated resistance to the drains is much lower than the resistance to the ditch.

The calibrated van Genuchten parameters are displayed in table 5.4. In this table also the van Genuchten parameters obtained by the evaporation method and the van Genuchten parameters from the Staringreeks are shown. The Staringreeks is a database for the average van Genuchten parameters of all Dutch topsoils and subsoils (Wösten *et al.*, 2001). Figures 5.5 and 5.6 show the soil water retention curves and the hydraulic conductivity curves respectively, by using these parameters. The soil water retention functions obtained

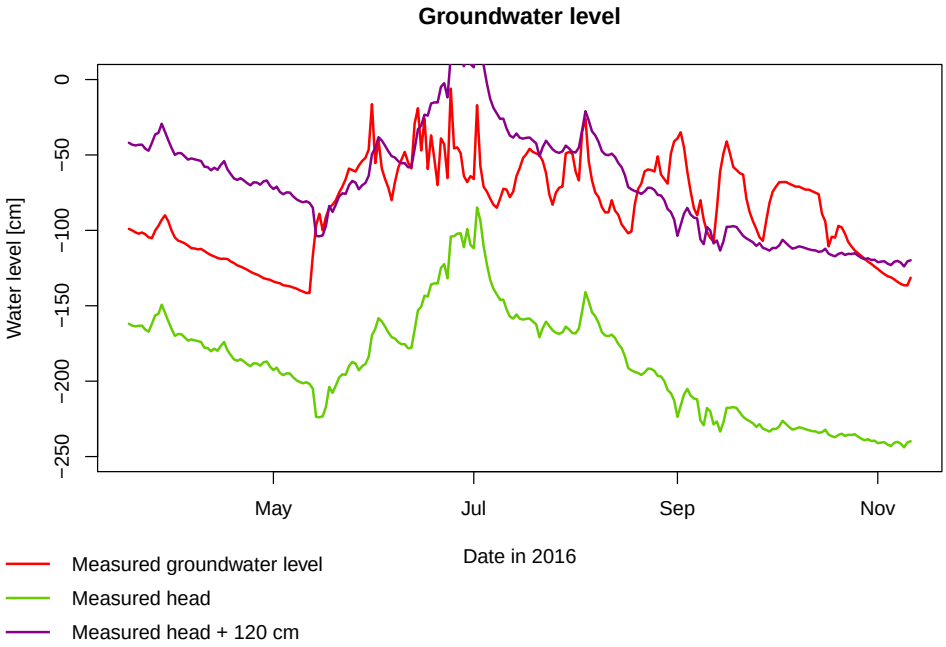

Figure 5.1: The measured groundwater level and the measured hydraulic head at 5m below surface. In this figure also the measured hydraulic head + 120 cm is shown, which is the calibrated hydraulic head.

Table 5.3: The calibrated irrigation water temperature. Between the dates the temperature is linearly interpolated.

Date	Temperature [°C]
1 Jan	17
1 Apr	17
1 May	20
15 Jul	23
1 Oct	20
1 Nov	17
31 Dec	17

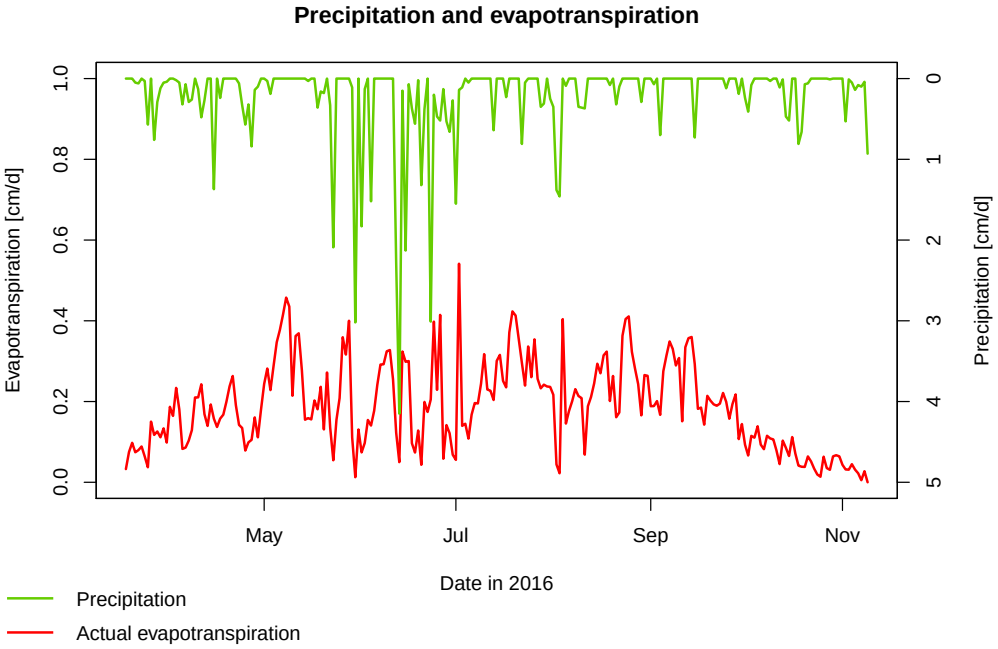

Figure 5.2: The precipitation and actual evapotranspiration in 2016.

from the evaporation method differ much from the calibrated soil water retention functions. The calibrated functions correspond at all depths more to the Staringreeks functions than to the functions from the evaporation method. At 20 cm depth, it seems that the staringreeks shows a soil water retention function for a less coarse material than the calibrated function. Therefore apparently the coarseness of the soil was higher than topsoil B2, which was used in the Staringreeks. At 40 cm depth, the Staringreeks and the calibrated function correspond well to each other. At 60 cm depth, the Staringreeks and calibrated function corresponds also well, except for the overestimated θ_{res} in the Staringreeks. The hydraulic conductivity obtained by calibration cannot be compared to the Staringreeks, as λ and K_{sat} are important parameters in the hydraulic conductivity and they are not calibrated. At 40 cm depth, the hydraulic conductivity of the evaporation method (and thus of the calibration) increases with increasing pressure head, which is physically impossible.

The simulated soil moisture contents and the groundwater levels before calibration and after the final calibration are shown in figure 5.7. The soil water content corresponds after calibration good to the measurements. The groundwater level corresponds fairly good

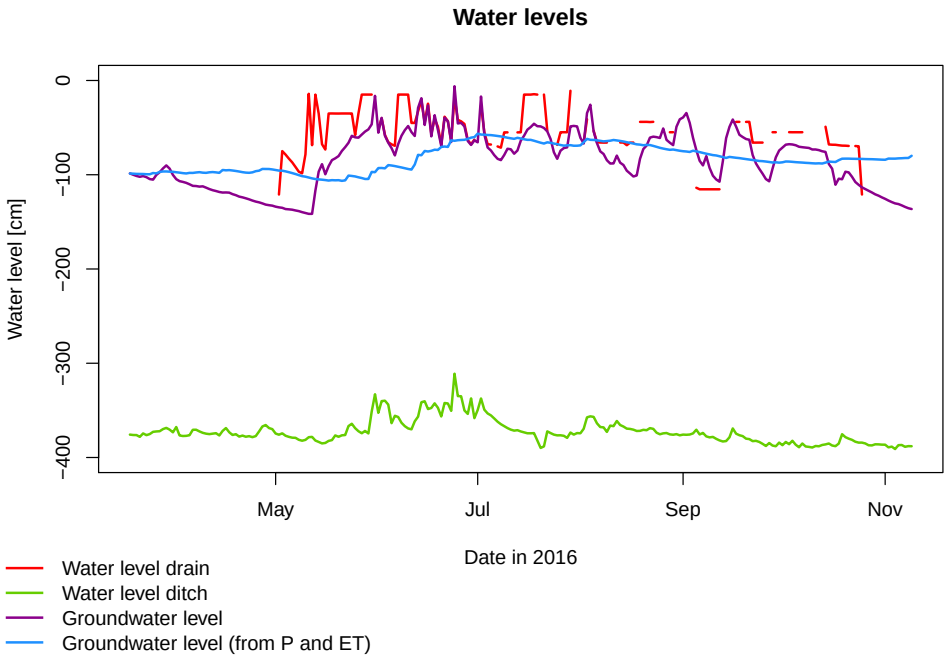

Figure 5.3: The groundwater level, the water level in the ditch and the water level in the drain. Also the hypothetic groundwater level if only precipitation and evapotranspiration would influence the groundwater level is shown.

Table 5.4: The van Genuchten parameters obtained for three depths (20, 40 and 60 cm below surface) of the study area. The parameters shown here are from three sources: the parameters obtained by the evaporation method (abbreviated: evaporation), the calibrated parameters and parameters from literature, from the Staringreeks (Wösten *et al.*, 2001). For 20 cm depth, the Staringreeks topsoil B2 is used and for 40 and 60 cm depth the Staringreeks subsoil O2 is used.

Depth	Source of parameter	θ_{res}	θ_{sat}	α	n	m	λ	K_{sat}
[cm]		[cm^3/cm^3]	[cm^3/cm^3]	[1/cm]	[-]	[-]	[-]	[cm/d]
20	evaporation	0.12	0.39	0.01	2.86	0.65	-0.63	2.67
	calibration	0.00	0.38	0.02	2.50	0.60	-0.63	2.67
	Staringreeks	0.02	0.42	0.03	1.49	0.33	-1.06	12.52
40	evaporation	0.13	0.39	0.01	1.95	0.49	-7.09	14.76
	calibration	0.02	0.36	0.03	2.20	0.55	-7.09	14.76
	Staringreeks	0.02	0.38	0.04	1.95	3.03	0.17	12.68
60	evaporation	0.00	0.26	0.01	3.19	0.69	-1.16	4.40
	calibration	0.10	0.40	0.04	3.50	0.71	-1.16	4.40
	Staringreeks	0.02	0.38	0.04	1.95	0.49	0.17	12.68

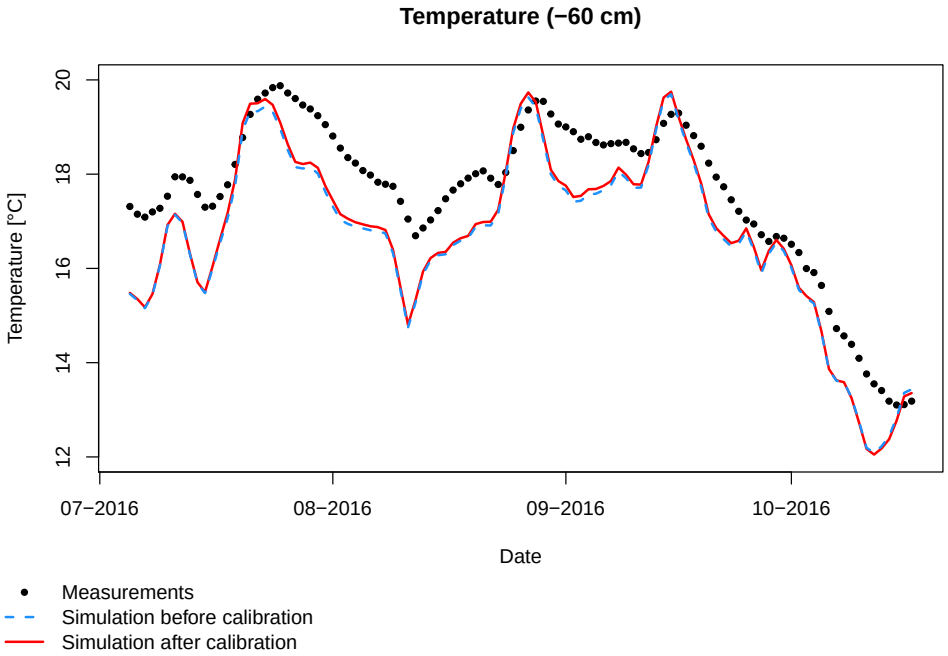

Figure 5.4: The simulated soil temperature before and after the calibration at a depth of 60 cm. Also the soil temperature measurements are shown.

to the measurements. What strikes is that at all depths the soil water content is underestimated in September and October. Besides, at 60 cm depth, the soil water content is overestimated before the start of the subirrigation, in April. In April also the groundwater table is overestimated.

The irrigation water temperature was difficult to calibrate, because of the relative short period of measurements. Before the calibration the water temperature was fixed at 20 °C. After the calibration the water temperature varies over the year, as is shown in table 5.3. In the winter it is expected that the irrigation temperature is lower than this calibrated 17 °C, because of the low air temperature. The difference in simulated soil temperature before and after the calibration, at 60 cm depth, is shown in figure 5.4. Apparently the calibration of the temperature barely affects the simulated soil temperature. Besides, the soil temperature is systematically underestimated by the simulations.

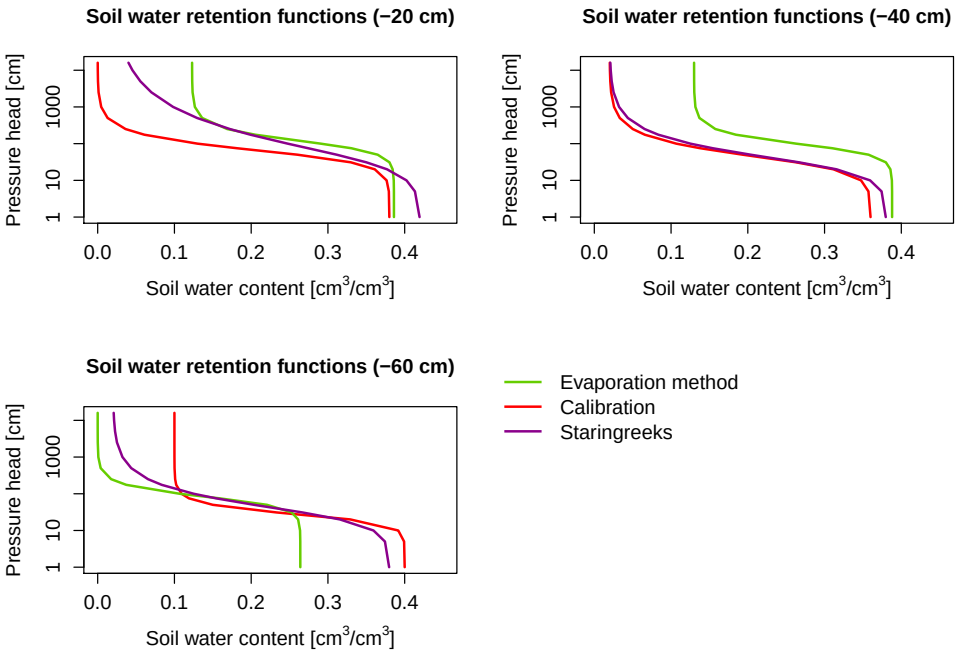

Figure 5.5: The soil water retention functions obtained by the evaporation method, calibration and the Staringreeks. The functions are shown for three depths. For 20 cm depth, the Staringreeks topsoil B2 is used and for 40 and 60 cm depth the Staringreeks subsoil O2 is used.

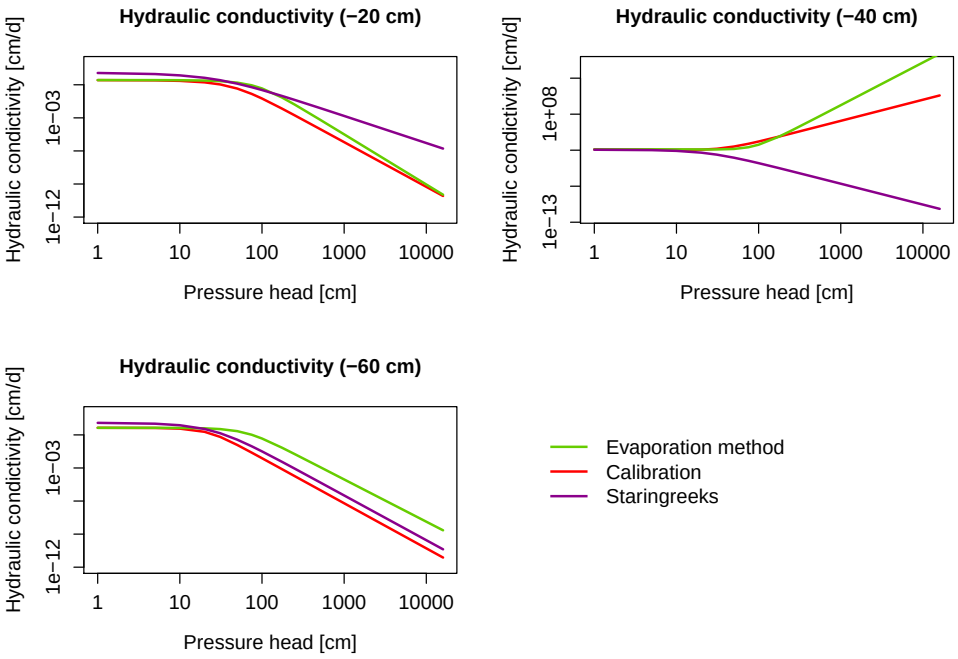

Figure 5.6: The hydraulic conductivity obtained by the evaporation method, calibration and the Staringreeks. The functions are shown for three depths. For 20 cm depth, the Staringreeks topsoil B2 is used and for 40 and 60 cm depth the Staringreeks subsoil O2 is used. The y axes of these plots have a different scale.

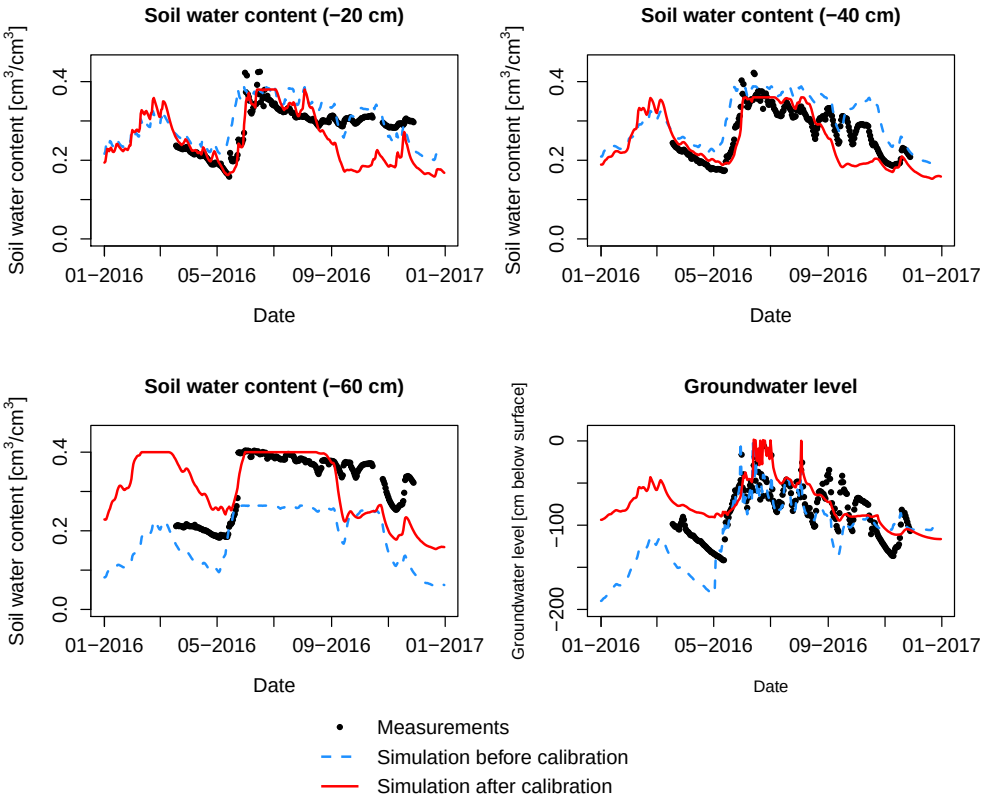

Figure 5.7: The simulated soil water content and groundwater level before and after the calibration. The soil water content is shown here for three depths. Also measurements of the soil water content and groundwater level are shown.

5.3 Optimal irrigation water head

Table 5.5 shows the obtained optimal irrigation head for every two months for every scenario. Table 5.6 shows the amount of subirrigation needed for these optimal heads. For the interpretation of the optimal irrigation heads, the differences in crop growth and stresses between the scenarios should be inspected. To compare the different scenarios, the irrigation head should be the same for all scenarios. Figure 5.8 shows the crop yield for all scenarios with a same irrigation head. This figure shows the yield for a situation with subirrigation and a situation without subirrigation. Table 5.7 gives an overview of the crop yields with irrigation and without irrigation.

It is remarkable from table 5.5 that grass needs subirrigation in November and December, as it is expected that the precipitation surplus in the winter is enough for the grass. Maize needs only subirrigation from May till August, which covers the whole growing period of maize. Strikingly, potatoes do not need subirrigation in May and June, although these months are part of their growing period. Besides, potatoes need less irrigation water per year than maize and grass. In 2050, more subirrigation is needed than at this moment.

The non smooth end of the crop yield for maize and potatoes (figure 5.8) is because the harvest date changes with the years, depending on the temperature and the yield in the figure is an average of 10 years. This figure also shows that the grass yield decreases in the beginning of the winter. With subirrigation, the yield of grass will be higher in the future than at this moment, which can also be seen in table 5.7. This table also shows that maize and potatoes have a relatively small increase in yield when subirrigation is applied, compared to grass.

Figure 5.9 shows the drought stress for the different scenarios, with and without subirrigation. Apparently only potatoes have a large drought stress. For all scenarios, the drought stress is significantly reduced by using subirrigation. Figure 5.10 shows the drought stress for a relatively dry year. Especially the drought stresses for 2006-2016 are larger in a relatively dry year. With subirrigation these large drought stresses are considerably reduced.

Figure 5.11 shows the oxygen stress for the different scenarios. It is remarkable that for grass the wet stress decreases when subirrigation will be used. The wet stress remains the same for maize and potatoes.

Table 5.5: The optimal irrigation heads for every scenario. The irrigation heads were determined for every two months. The drains are at a depth of 120 cm below surface, so an irrigation head of -120 cm corresponds to a situation without irrigation.

Months	Grass 2006-2016	Maize 2006-2016	Potatoes 2006-2016	Grass 2050 Gh	Grass 2050 Gl	Grass 2050 Wh	Grass 2050 Wl
	[cm]	[cm]	[cm]	[cm]	[cm]	[cm]	[cm]
Jan-Feb	-120	-120	-120	-90	-90	-120	-120
Mar-Apr	-90	-120	-90	-90	-90	-90	-90
May-Jun	-90	-60	-120	-60	-60	-60	-60
Jul-Aug	-60	-90	-30	-60	-60	-60	-60
Sep-Oct	-120	-120	-120	-60	-60	-120	-120
Nov-Dec	-60	-120	-120	-90	-90	-90	-30

Table 5.6: The irrigation flux per year, averaged over 10 years. This irrigation flux is shown for the different scenarios.

Scenario	Irrigation flux
	[cm/yr]
Grass (2006-2016)	40.9
Maize (2006-2016)	38.0
Potato (2006-2016)	22.7
Grass (2050 Gh)	52.5
Grass (2050 Gl)	50.6
Grass (2050 Wh)	41.4
Grass (2050 Wl)	64.4

Table 5.7: The yield with subirrigation, the yield without subirrigation and the increase in yield by using subirrigation. In here the yields are shown for the parts of the plant which are useful (blades of grass, maize cob and the potato itself).

Scenario	Increase yield
	[%]
Grass (2006-2016)	3.5
Maize (2006-2016)	1.6
Potato (2006-2016)	1.1
Grass (2050 Gh)	5.6
Grass (2050 Gl)	3.0
Grass (2050 Wh)	7.7
Grass (2050 Wl)	4.1

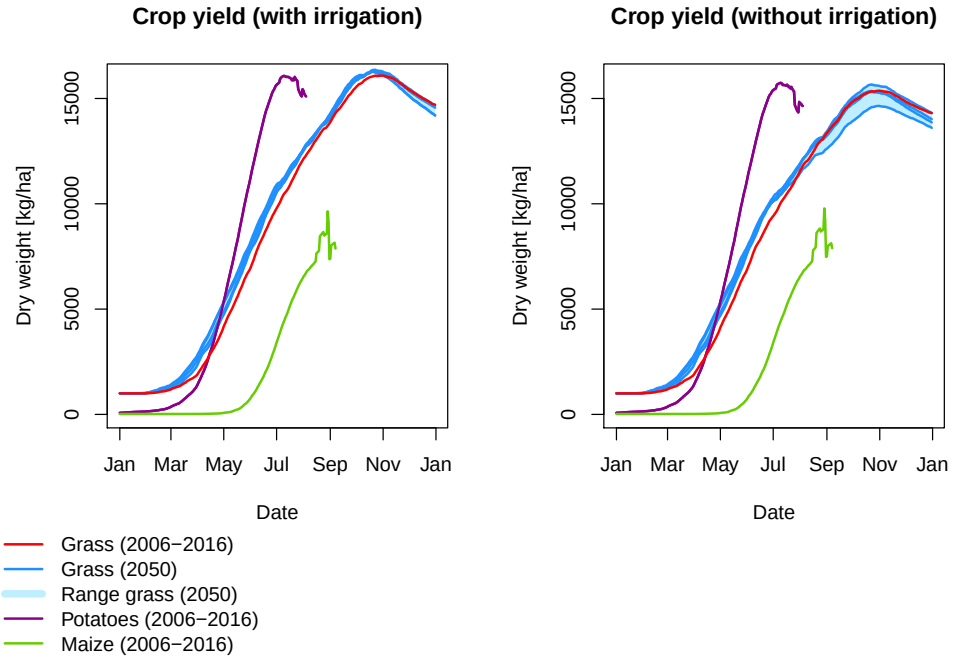

Figure 5.8: The simulated crop yield for every scenaro, both for a situation with and a situation without subirrigation. The yield of all simulated years is averaged to one year. For every scenario the optimal irrigation heads obtained for grass (2006-2016) are used to make the comparison easier. For grass (2050), the different climate scenarios are plotted. The yield range of the scenarios is also displayed in the graph.

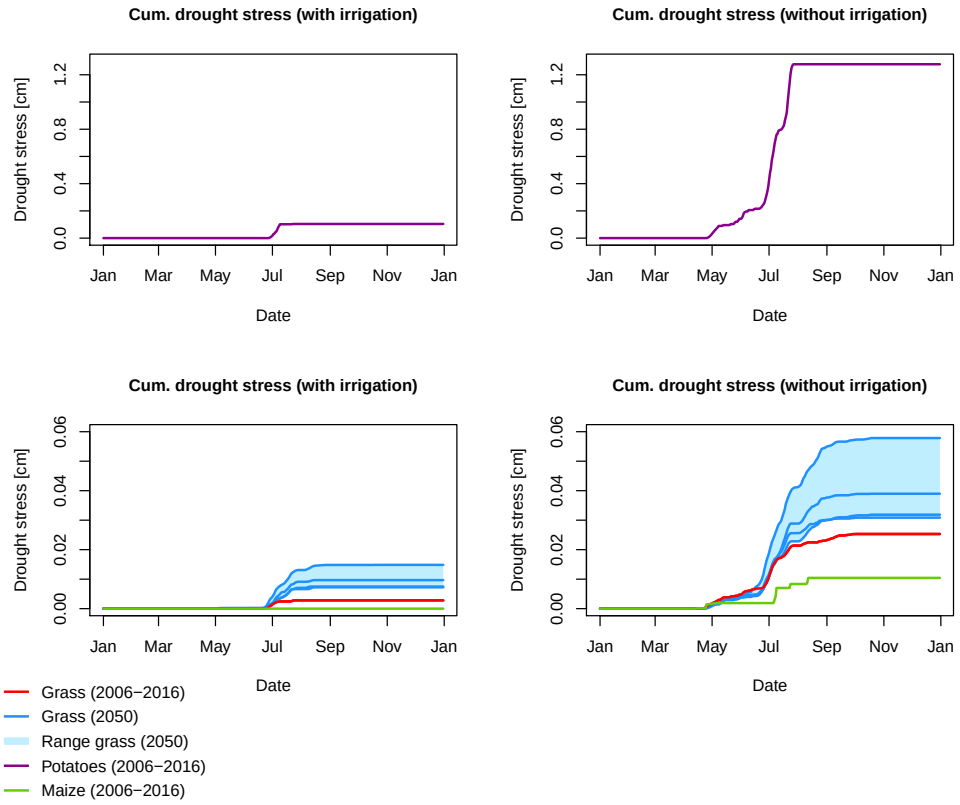

Figure 5.9: The simulated cumulative drought stress for every scenaro, both for a situation with and a situation without subirrigation. The drought stress of all simulated years is averaged to one year. For every scenario the optimal irrigation heads obtained for grass (2006-2016) are used to make the comparison easier. For grass (2050), the different climate scenarios are plotted. The stress range of the scenarios is also displayed in the graph. Because of the large difference in stresses, the drought stress of potatoes is plotted in a separate graph.

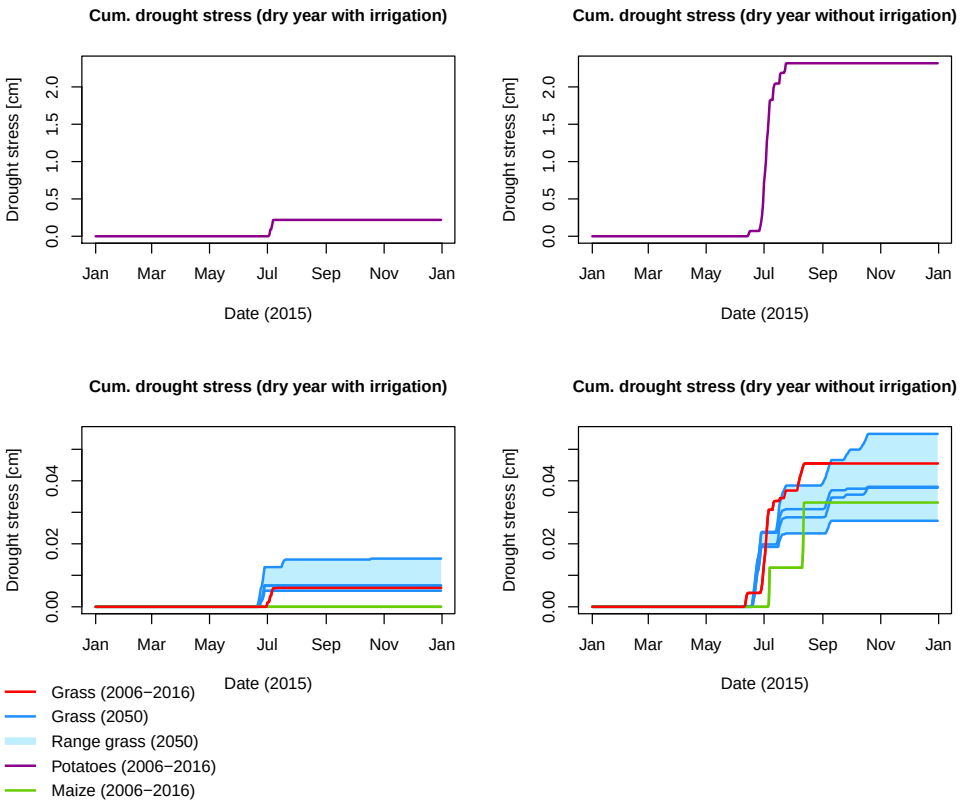

Figure 5.10: The simulated cumulative drought stress for a relatively dry year, both for a situation with and a situation without subirrigation. 2015 is used as dry year and for climate change, a relatively dry 2050 year is used. For every scenario the optimal irrigation heads obtained for grass (2006-2016) are used to make the comparison easier. For grass (2050), the different climate scenarios are plotted. The stress range of the scenarios is also displayed in the graph. Because of the large difference in stresses, the drought stress of potatoes is plotted in a separate graph.

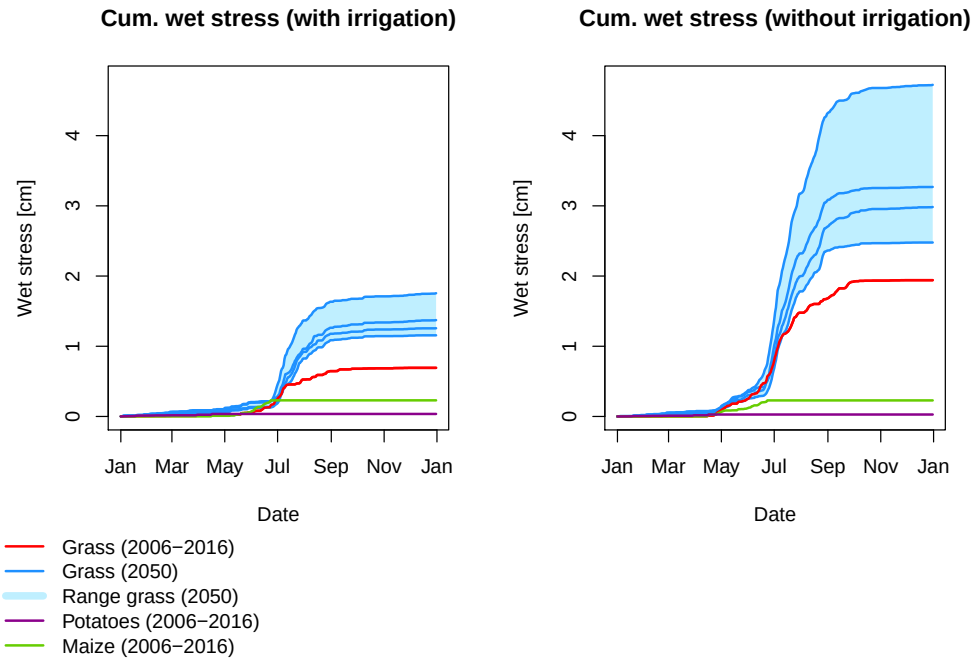

Figure 5.11: The simulated cumulative wet stress for every scenaro, both for a situation with and a situation without subirrigation. The wet stress of all simulated years is averaged to one year. For every scenario the optimal irrigation heads obtained for grass (2006-2016) are used to make the comparison easier. For grass (2050), the different climate scenarios are plotted. The stress range of the scenarios is also displayed in the graph.

5.4 Soil temperature

The measurements of the soil temperature are shown in the figures 5.12, 5.13 and 5.14. Figures 5.12 and 5.14 show only measurements at time when there was subirrigation, while figure 5.13 shows also measurements while there was no subirrigation, so that differences between irrigation times and times without irrigation become clear. The measurements of all depths show that it is most of the time warmer near the drain than 4 m from the drain, although most of the time of the month August this statement is not true. Figure 5.13 shows a clear difference in temperature above the drain and 4 m from the drain when there is subirrigation. This difference is not clear anymore when there is no subirrigation (after 13 October), which is because then there is no subirrigation so the extra heat source is not there anymore.

The linear regression shows that it is significantly (90% confidence interval) warmer directly above the drain than at a distance of both 2 and 4 m from the drain. This is true for the depths 40 and 60 cm. At 20 cm below surface this relation was not significant. The graphs of this linear regression can be found in appendix D.

The output of the multiple linear regression is shown in table 5.8. In here the regression coefficients are shown which have a significant (90% confidence interval) influence on the temperature difference due to subirrigation. This multiple linear regression is done for the difference between temperature measured at a certain depth directly above the drain and at the same depth 2 m from the drain. In the regression also measurements above the drain are compared with measurements 4 m from the drain. It was expected that the regression coefficients of drain temperature, air temperature, drain pressure and drain flux are all positive, because they contribute to a higher soil temperature near the drain. Most of them are indeed positive, but not all.

Figure 5.15 shows the SWAP soil temperature simulations at 40 and 120 cm depth. The simulations are done for the current situation, with and without simulating of the extra heat flux caused by subirrigation. These simulations show that it is at 40 and 120 cm depth always warmer when the heat flux coming from the drain is simulated than when it is not simulated. Especially in July, August, November and December this difference is large, with a maximum of 1.8°C difference. Figure 5.16 also shows the simulation with and without simulating of the extra heat flux, but this figure shows a depth profile of the soil temperature. SWAP simulations with the extra heat flux result in a higher temperature than simulations with-

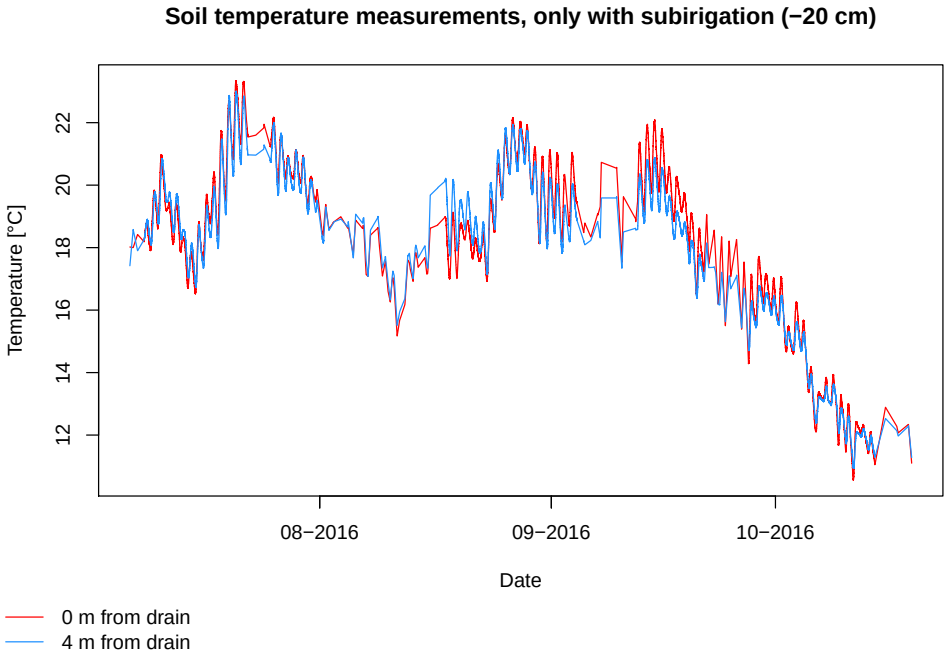

Figure 5.12: The measured soil temperatures at 20 cm depth, directly above the drain and 4 m from the drain. Only measurements at times when there was subirrigation are displayed.

out the extra heat flux. This difference in temperature is higher when going deeper in the soil profile. Besides, the soil temperatures simulated with different irrigation water temperatures diverge when going deeper in the profile. To inspect the influence of the drainage temperature in further detail, figure 5.17 shows the depth profile of soil temperatures when using different (extreme) irrigation temperatures. Also here the soil temperature diverges when going deeper in the profile.

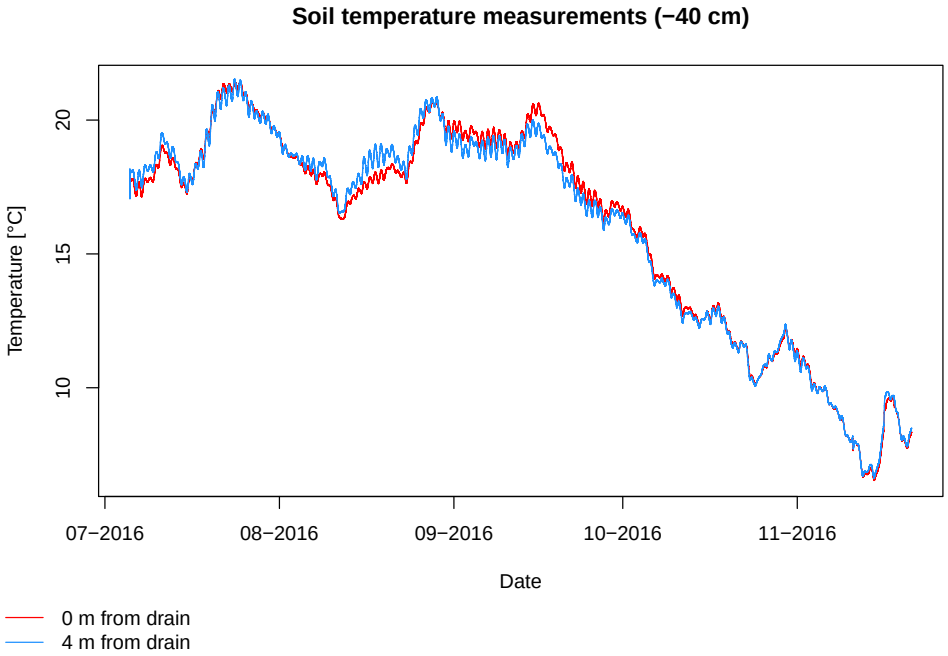

Figure 5.13: The measured soil temperatures at 20 cm depth, directly above the drain and 4 m from the drain. In here all measurements are shown, so also measurements at times without subirrigation. At 13 October, the subirrigation was turned off.

Table 5.8: The outcome of the multiple linear regression of the soil temperature measurements. At each depth measurements directly above the drain are compared with measurements at the same depth, but at a horizontal distance of 2 and 4 m from the drain. The numbers in the table are the multipliers of the variables to come to the temperature difference between two measurements.

Depth sample [cm]	Compared distances from drain [cm]	Intercept [-]	Drain pressure [0.1 cm^2/N]	Drain temperature [1/T]	Drain flux [h/m^3]	Air temperature [1/T]	Radiation [cm^2 h/J]
20 cm	0 - 200	0.458	7.732	-0.056		0.034	
	0 - 400	-0.949	6.984			0.050	
40 cm	0 - 200	-0.986	7.265	0.058	-0.003	0.018	-0.050
	0 - 400	-1.525	7.274	0.079	-0.002	0.008	0.099
60 cm	0 - 200	-1.167	7.389	0.084	-0.002	0.004	
	0 - 400	-1.454	7.584	0.086			0.028

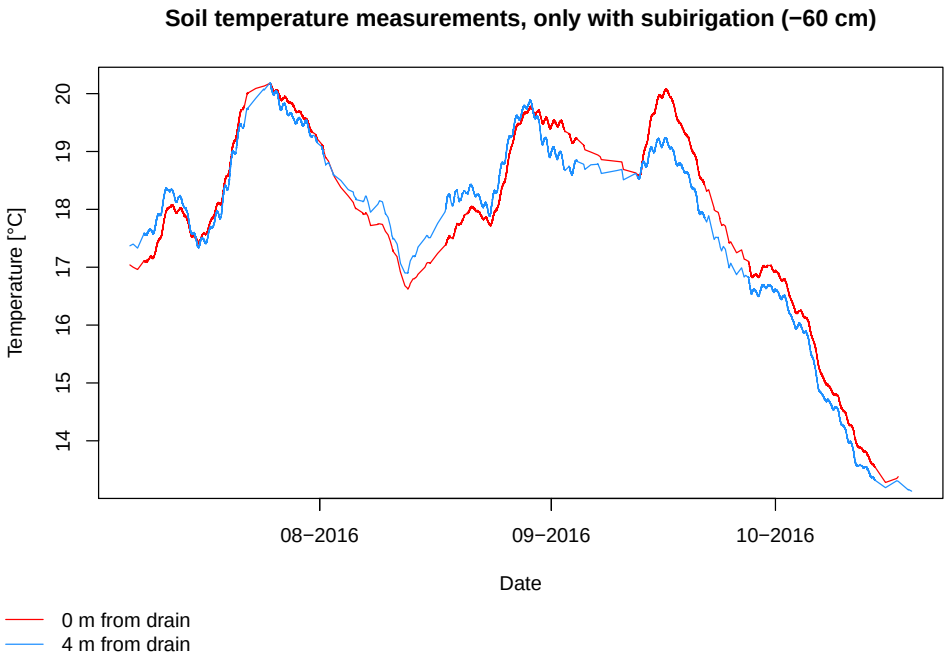

Figure 5.14: The measured soil temperatures at 60 cm depth, directly above the drain and 4 m from the drain. Only measurements at times when there was subirrigation are displayed.

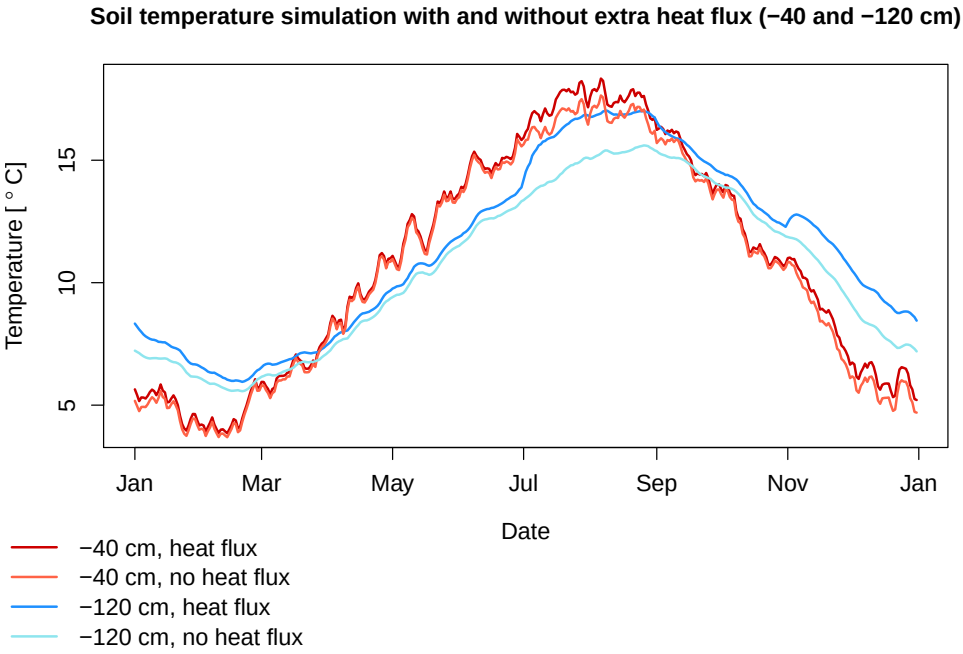

Figure 5.15: The simulated soil temperatures at 40 and 120 cm depth for grass (2006-2016) by the SWAP model. The simulations were done with and without the simulation of the extra heat source, caused by the subirrigation. The soil temperatures of all simulated years were avered to one year. For these simulations the optimal irrigation heads for grass (2006-2016 are used).

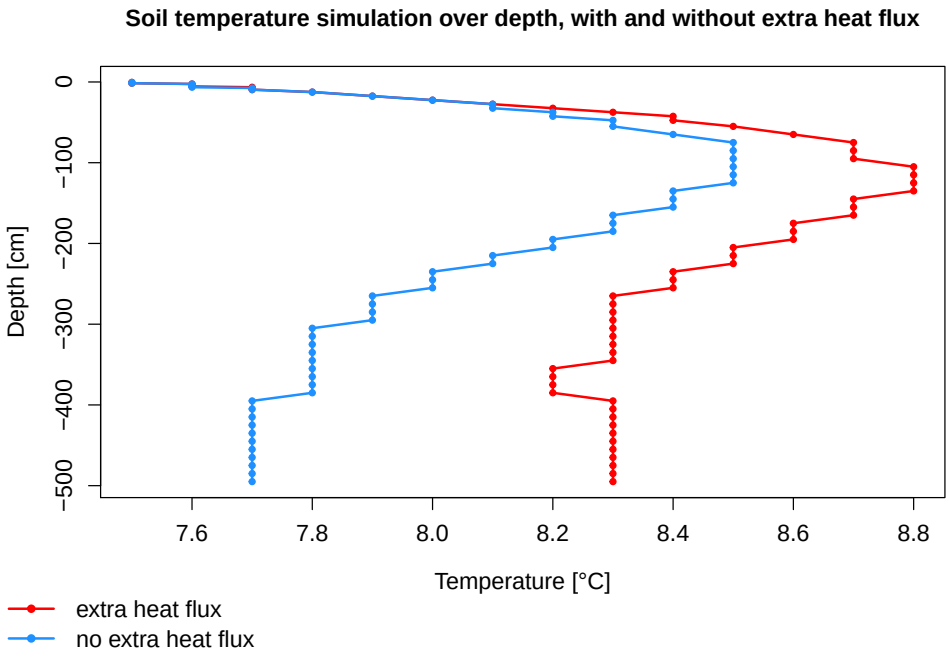

Figure 5.16: The simulated soil temperatures over the whole soil profile for grass (2006-2016) by the SWAP model. The simulations were done with and without the simulation of the extra heat source, caused by subirrigation. This simulated temperatures belong to May 1st, 2015. For these simulations the optimal irrigation heads for grass (2006-2016 are used. The graph is angular because the simulated temperatures have an accuracy of 0.1 °C. The dots are added in the graph to clarify this effect.

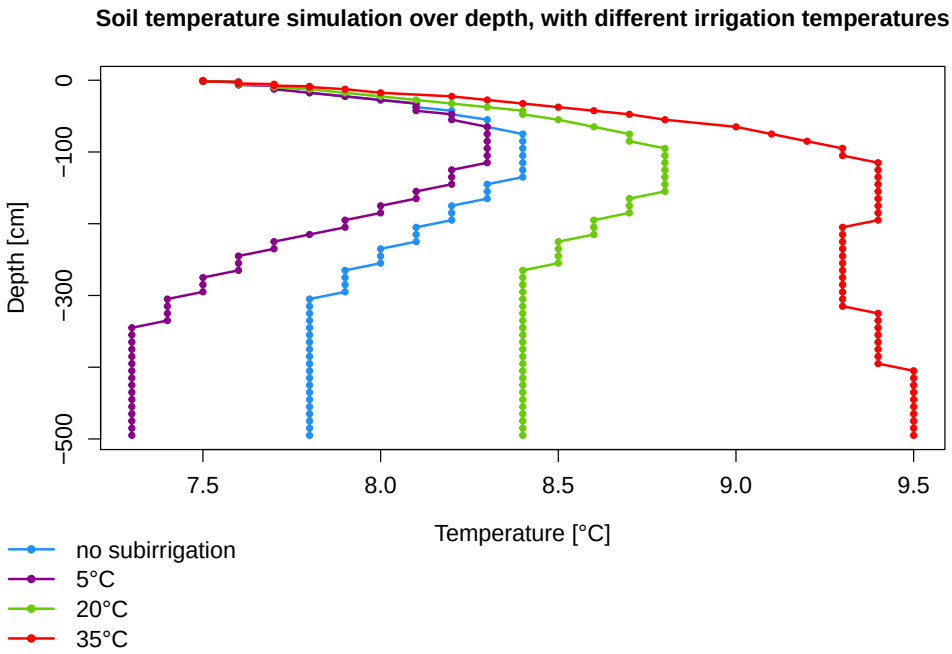

Figure 5.17: The simulated soil temperatures over the whole soil profile for grass (2006-2016) by the SWAP model. The simulations were done with and without subirrigation and with different irrigation water temperatures. This simulated temperatures belong to May 1st, 2015. For these simulations the optimal irrigation heads for grass (2006-2016 are used. The graph is angular because the simulated temperatures have an accuracy of 0.1 °C. Therefore the dots are added in the graph to clarify this effect.

Chapter 6

Discussion

6.1 Calibration and evaporation method

Figure 5.7 shows the results of the calibration of soil water content and groundwater level. For the calibration, the measured hydraulic head 5 meter below surface is increased by 1.20 m to have a correct simulated irrigation flux. Figure 5.1 shows that this increased head corresponds at times with subirrigation to the measured groundwater level. This can be explained by the loamy layer, which is shown in figure 6.1. This figure also shows the depth of the drains. The bottom of this figure is the depth where the measurements of the hydraulic head were taken. In the study area there is downward seepage. The loamy layer works as a resistance for the downward seepage. Therefore the water has difficulties with passing the loamy layer, which will cause an hydraulic head underneath the layer which is lower than in a situation without loamy layer. Therefore this head had to be increased in order to corresponds to the situation above the loamy layer. Without subirrigation, there is less downward seepage and therefore the increased head is higher than the groundwater measurements before the subirrigation is used (before May).

Figure 5.7 shows that after the calibration, in September and October the soil water content is underestimated. This can possibly be caused by the low amount of measurements in those two months of the water level in the supply well, which corresponds to the irrigation head inside the drains (see figure 5.3). Therefore the amount of days with subirrigation can be underestimated and with less subirrigation, a lower soil water content is simulated. At 60 cm depth, the soil moisture content is overestimated in April. In April also the groundwater level is overestimated. This can be caused by the overestimated hydraulic head at the bottom of the SWAP model (see figure 5.1). This overestimated head causes an overestimation

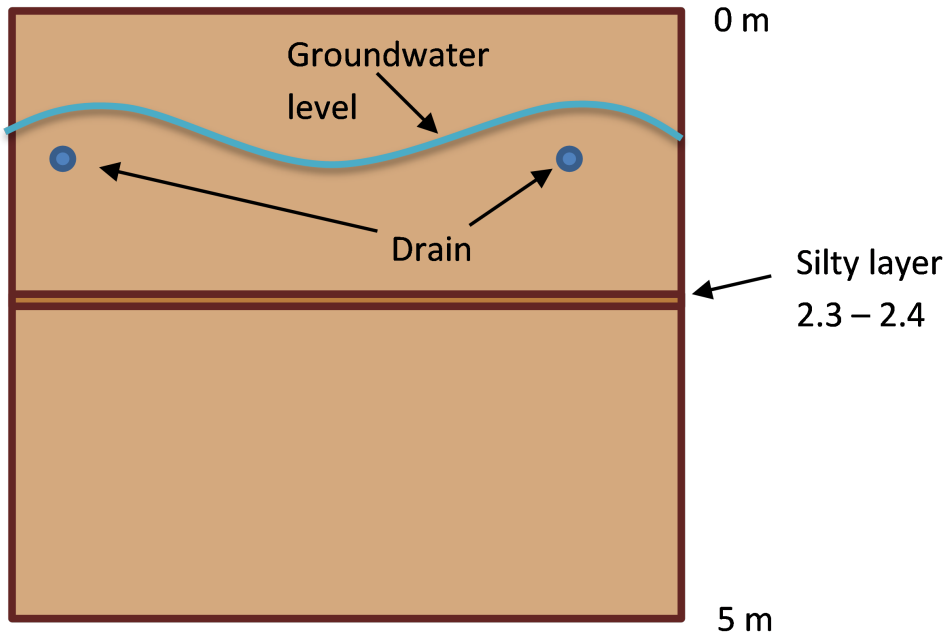

Figure 6.1: An overview of the soil profile until 5m depth, with the silty layer. Also the locations of two drains are shown and the groundwater level is shown.

in groundwater level and therefore at a certain depth an overestimation in the soil water content. Overall, the calibrated parameters of soil water content and groundwater level are fairly good representative for the real situation, but care should be taken that the calibrated parameters do not perfectly match the real situation.

The soil water retention functions obtained by the evaporation method, calibration and by literature (the Staringreeks) are shown in figure 5.5. The Staringreeks corresponds better to the calibrated soil water retention functions than the functions obtained by the evaporation method. Besides, the obtained hydraulic conductivity at 40 cm depth by the evaporation method is physically not possible (figure 5.6). This hydraulic conductivity is caused by the large differences in λ and K_{sat} between the different soil samples at 40 cm depth, of which the average is taken. Therefore it was better if the hydraulic conductivity was also calibrated in the SWAP model.

In the analysis of the evaporation method, a lot of choises have been made. There had to be determined which tensiometers were taken into account, what the ending point is of the measurements. Besides, in the filter step the band width, the minimum timestep and the minimum $\frac{dh}{dz}$ should be determined. In the fit step the modality,

the used mean and the place of fixation of the water content should be determined. All these decisions have influence on the outcome of the evaporation method. There are no strict rules for these decisions to follow so experience is needed to make the best decisions. In this research all options are tried and the best results are selected. The fact that the parameters from the evaporation method do not match with the parameters from the calibration and from literature can be caused by the large amount of decisions based on experience made by the evaporation method. So the SWAP model could better be calibrated by using the parameters of the Staringreeks than the evaporation method as initial values. On the basis of this research, it can be concluded that the evaporation method is not reliable for obtaining the van Genuchten parameters.

The calibration of the irrigation temperature is shown in figure 5.4. In here the calibration barely affects the soil temperature. This is possibly because the soil temperature is mainly affected by the air temperature and the temperature of the groundwater level. The irrigation temperature affects the soil temperature only minor. Therefore, a change in irrigation temperature of a few degrees centigrate has little effect on the soil temperature. Figure 5.4 also shows that the soil temperature is underestimated by the SWAP model. This can possibly be because the temperature sensors are installed somewhat higher than at 60 cm depth. As the soil temperature decreases with depth, this can cause the measured temperature to be higher than the temperature at 60 cm depth. Another possible reason for the underestimation of the soil temperature is that SWAP takes the field-averaged soil temperature. The measurements shown in figure 5.4 are the average of measurements directly above the drain, at 2 and at 4 m from the drain. This can be different from the field-averaged soil temperature.

6.2 Optimal irrigation water head

Figure 5.8 shows the crop yield of the different scenarios. In November and December the crop yield of grass decreases again. In these months also the rooting depth of grass decreases. Therefore probably grass has difficulties with extracting the soil water and it has benefit from subirrigation. Therefore grass needs subirrigation in November and December. In 2050 grass needs more subirrigation than at this moment (table 5.5 and table 5.6). This can be caused by the extension of the growing season due to temperature increase. In January, February, September and October the climate scenarios

Wh and Wl do not need subirrigation, while the climate scenarios Gh and Gl need subirrigation. The climate scenarios Wh and Wl have the highest increase in extreme precipitation in the winter (Klein Tank *et al.*, 2015). For autumn, no extensive precipitation analyses was done. The increase in extreme precipitation in winter causes wet stress and therefore subirrigation is not needed, while it is needed in scenarios with less extreme precipitation. The climate scenario Wl needs a much higher irrigation head in November and December than the other climate scenarios (see table 5.5). It is not clear what the cause is for this. Maybe it is because of the large decrease in days with precipitation for scenario Wl, compared to the current climate (Klein Tank *et al.*, 2015).

The increase in yield by using subirrigation is only 1.6% and 1.1% for maize and potatoes, while for grass it is 3.5% (see table 5.7). This is possibly due to the larger root depth of maize and potatoes in comparison with grass. The increase in yield by using subirrigation is 5.6%, 3.0%, 7.7% and 4.1% for the climate scenarios Gh, Gl, Wh and Wl respectively. This is very similar to the increase in potential evapotranspiration of 5%, 3%, 7% and 4% for the scenarios Gh, Gl, Wh and Wl respectively. This is because an increase in evapotranspiration might cause a soil water shortage in the rooting zone. Subirrigation decreases this shortage and therefore the difference in yield with and without subirrigation is higher.

Figure 5.11 shows the wet stress for the different scenarios. It is unknown why for grass the wet stress decreases when subirrigation will be used. A possible explanation is that subirrigation causes a larger growth of grass. Therefore the grass extracts more water from the soil with subirrigation. This causes a relatively less wet soil than in the situation without subirrigation. And therefore the wet stress is lower in the situation with subirrigation. Further research should investigate if this theory is correct.

6.3 Soil temperature

It is remarkable that the temperature sensors measured in August a higher temperature further from the drain than directly above the drain. This can only be caused by a colder irrigation temperature than soil temperature. The colder irrigation temperature might be caused by the relatively cold air temperatures in August, which will cause a cooling of the irrigation temperature when the irrigation water is transported to the study area and when it is stored in the collection well. This relatively cool irrigation water should be colder

than the relatively warm soil temperature in the end of the summer, which causes a soil temperature decrease due to subirrigation.

When looking at the linear regression, it can be concluded that it is warmer near the drain than at 2 or 4 m from the drain (see appendix D). This is only significant (90% confidence interval) at 40 and 60 cm depth. Therefore the irrigation water causes an increase in soil temperature. This increase in soil temperature can extend the growing season. The parts where the measured irrigation temperature is colder near the drain than 4 m from the drain can be declared by multiple linear regression, because the difference in temperature is not always the same and can be declared by multiple variables. The results from this regression are given in table 5.8. It was expected that the regression coefficients of drain temperature, air temperature, drain pressure and drain flux are all positive, because they contribute to a higher soil temperature near the drain. Most of them are indeed positive, but not all. A possible explanation for the negative coefficients is that the temperature of the drain water also reaches the temperature sensor further away and therefore the difference in the measured temperature between the two sensors will become smaller. This is schematically shown in figure 6.2. Further on, it is remarkable that the radiation is once negatively correlated and twice positively. An explanation for the negative correlation could be that the daily range in temperature is smaller near the drain than far from the drain, because of the influence of the drain water. This concept is shown in figure 6.3. Due to this concept, the temperature difference is higher during the night than during the day, which gives a negative correlation coefficient. A possible explanation for the positive correlation could be that the sun is warming the water in the supply well and this causes a higher drain temperature during the day than during the night.

The SWAP simulations show that it is at 40 and 120 cm depth always warmer when the heat flux coming from the drain is simulated than when it is not simulated, see figure 5.15. For this figure the optimal irrigation heads for grass at 2006-2016 are used. The large temperature differences with and without extra heat flux in July, August, November and December are caused by the large irrigation heads in these months, which increases the effect of the irrigation temperature on soil temperature.

Figures 5.16 and 5.17 show how the soil temperature changes over depth. The difference in soil temperature becomes larger when going deeper in the soil. This is caused by the soil temperatures which are influenced by the radiation and the drain temperature. Therefore, the deeper in the profile the more the drain temperature

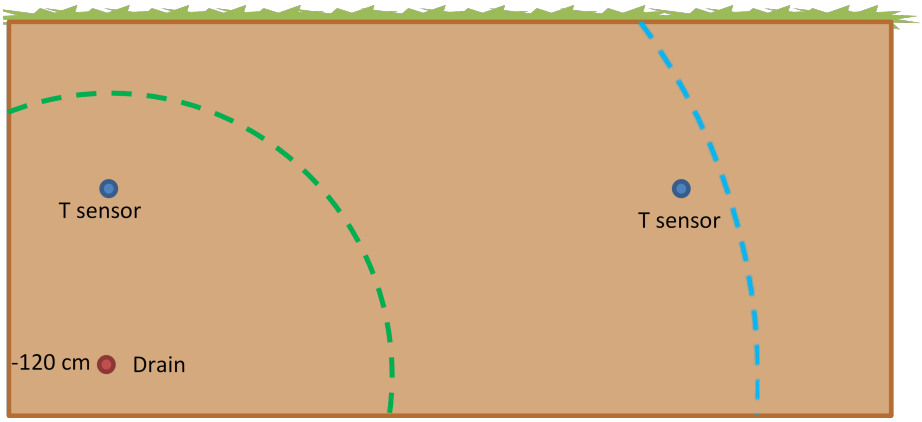

Figure 6.2: Two temperature sensors are shown: one above the drain and one at a distance from the drain. If the temperature influence from the irrigation water on the soil temperature is displayed by the area within the green circle, only the first sensor will measure an increase in temperature. When the temperature influence from the drain is displayed by the blue circle, both sensors will measure the influence of the irrigation temperature and the temperature difference between the two sensors will be smaller.

influences the soil temperature.

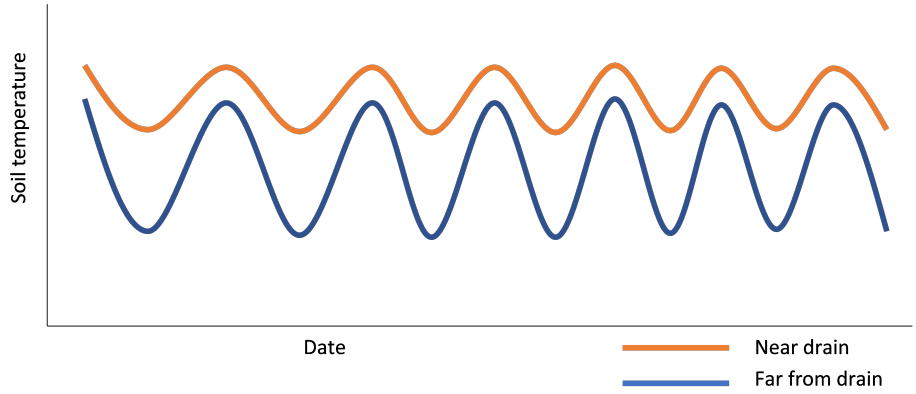

Figure 6.3: An overview of possible temperature measurements near the drain and far from the drain. As can be seen, the temperature difference between the two measurements is smaller when the soil temperature is high, so during the day, than during the night.

Chapter 7

Conclusion

The optimal irrigation heads for grass, maize and potatoes can be seen in table 7.1. Maize and potatoes need fewer periods in the year irrigation than grass. Besides, the increase in crop yield for maize and potatoes is much lower than the increase in crop yield for grass. Therefore it can be concluded that it adds value to use subirrigation at grassland, where the optimal irrigation heads are shown in table 7.1. So grass also needs subirrigation in the beginning of the winter. For maize and potatoes subirrigation does not add much value.

For grass the optimal irrigation heads for 2050 with climate change are shown in table 7.2. The grass yield will be higher in 2050 than it is at this moment. Furthermore, the yield increase by using subirrigation will also probably be higher in 2050, so irrigation will add more value in the future.

At 40 and 60 cm depth the soil is significant warmer near the drain than 2 or 4 m from the drain. Therefore the irrigation water temperature can extend the growing season. The difference in drain temperature near the drain and at 2 or 4 m from the drain can be described by drain temperature, air temperature, drain pressure, drain flux and radiation. The difference in soil temperature becomes larger when going deeper in the soil.

Concluding, the reuse of process water for subirrigation of grass is useful. It will reduce the drought stresses of grass. Besides, it will extend the growing season. Therefore the subirrigation with process water will cause a larger crop yield. In the future the subirrigation with process water will increase the yield even more. Therefore it is recommended to reuse process water for subirrigation on more locations in the Netherlands.

Table 7.1: The optimal irrigation heads for the different crop types. The irrigation heads were determined for every two months.

Months	Grass 2006-2016	Maize 2006-2016	Potatoes 2006-2016
	[cm]	[cm]	[cm]
Jan-Feb	-120	-120	-120
Mar-Apr	-90	-120	-90
May-Jun	-90	-60	-120
Jul-Aug	-60	-90	-30
Sep-Oct	-120	-120	-120
Nov-Dec	-60	-120	-120

Table 7.2: The optimal irrigation heads for every scenario. The irrigation heads were determined for every two months.

Months	Grass 2006-2016	Grass 2050 Gh	Grass 2050 Gl	Grass 2050 Wh	Grass 2050 Wl
	[cm]	[cm]	[cm]	[cm]	[cm]
Jan-Feb	-120	-90	-90	-120	-120
Mar-Apr	-90	-90	-90	-90	-90
May-Jun	-90	-60	-60	-60	-60
Jul-Aug	-60	-60	-60	-60	-60
Sep-Oct	-120	-60	-60	-120	-120
Nov-Dec	-60	-90	-90	-90	-30

Bibliography

Bakker, A, & Bessembinder, J. 2012. Time series transformation tool: description of the program to generate time series consistent with the KNMI '06 climate scenarios.

Bakker, G, Heinen, M, Wesseling, J G, de Groot, W J M, Assinck, F B T, & Hummelink, E W J. 2015. *Bodemfysische gegevens in BIS*. Tech. rept.

Bartholomeus, Ruud, Van Den Eertwegh, Gé, & Simons, Gijs. 2015a. *Anticipating on amplifying water stress: Optimal crop production supported by anticipatory water management*. Tech. rept. June.

Bartholomeus, Ruud, Eertwegh, Gé Van Den, & Simons, Gijs. 2015b. Naar online en optimale sturing van Klimaat Adaptieve Drainage. *Stromingen*, **24**(4), 27–42.

Bartholomeus, Ruud P. 2015. *Ontwerp sub-irrigatie Van Dijk / Bavaria*. Tech. rept. KWR Watercycle Research Institute.

Bartholomeus, Ruud P., & van Loon, A. 2017. Meetresultaten 2016 sub-irrigatie Van Dijk / Bavaria. 1–10.

Bartholomeus, Ruud P., Witte, Jan Philip M, van Bodegom, Peter M., van Dam, Jos C., & Aerts, Rien. 2008. Critical soil conditions for oxygen stress to plant roots: Substituting the Feddes-function by a process-based model. *Journal of Hydrology*, **360**(1-4), 147–165.

Bartholomeus, Ruud P, Heijkens, Joost, Droogers, Peter, van Dam, Jos C, & van Walsum, Paul. 2015c. Werkelijke verdamping in hydrologische modellen. *Pages 105–155 of: Verdamping in de hydrologie*.

Batlla, D., & Benech-Arnold, R. L. 2015. A framework for the interpretation of temperature effects on dormancy and germination in seed populations showing dormancy. *Seed Science Research*, **25**, 147–158.

Belmans, C., Wesseling, J. G., & Feddes, R. A. 1983. Simulation model of the water balance of a cropped soil: SWATRE. *Journal of Hydrology*, **63**(3-4), 271–286.

Black, TA, Gardner, WR, & Thurtell, GW. 1969. The prediction of evaporation, drainage, and soil water storage for a bare soil. *Soil Science Society of America Journal*, **33**(5), 655–660.

Boels, D, Van Gils, J B H M, Veerman, G J, & Wit, K E. 1978. Theory and System of automatic determination of soil moisture characteristics and unsaturated hydraulic conductivities. *Soil Science*, **126**(4).

Boesten, J.J.T.I., & Stroosnijder, L. 1986. Simple model for daily evaporation from fallow tilled soil under spring conditions in a temparate climate. *Netherlands Journal of Agricultural Science*, **34**, 75–90.

Bouten, Willem. 1992. *Monitoring and modelling forest hydrological processes in support of acidification research.* Universiteit van Amsterdam.

Braden, H. 1985. Ein energiehaushalts-und verdunstungsmodell for wasser und stoffhaushaltsuntersuchungen landwirtschaftlich genutzer einzugsgebiete. *Mitteilungen Deutsche Bodenkundliche Geselschaft*, **42**, 294–299.

Broks. 1989. *Geohydrologisch onderzoek winplaats Lieshout WOB.* Tech. rept. Broks Adviezen, 's Hertogenbosch.

Campbell Scientific. 1983. *Model 107 Temperature Probe.* Tech. rept.

Causton, D R, & Venus, J C. 1981. *The biometry of plant growth.* London: Edward Arnold.

CBS, PBL, & Wageningen UR. 2016. *Waterwinning en watergebruik in Nederland, 1976-2012.*

Colsen, J. 2012. PEKA-Kroef en Waterschap Aa en Maas slaan handen ineen voor een betere waterkwaliteit. *Neerslag*, **1**, 25–27.

Cook, F. J., Knight, J. H., & Kelliher, F. M. 2013. Modelling oxygen transport in soil with plant root and microbial oxygen consumption: Depth of oxygen penetration. *Soil Research*, **51**, 539–553.

Croda. 2014. Croda (Gouda) spaart grondwater met innovatief hergebruik van afvalwater. *H2O*, **47**(5), 24.

de Jong van Lier, Q., van Dam, J. C., Metselaar, K., de Jong, R., & Duijnisveld, W. H. M. 2008. Macroscopic Root Water Uptake Distribution Using a Matric Flux Potential Approach. *Vadose Zone Journal*, **7**(3), 1065.

Douma, Jacob C., Bardin, Vincent, Bartholomeus, Ruud P., & van Bodegom, Peter M. 2012. Quantifying the functional responses of vegetation to drought and oxygen stress in temperate ecosystems. *Functional Ecology*, **26**, 1355–1365.

Doussan, Claude, Pierret, Alain, Garrigues, Emmanuelle, & Pagès, Loïc. 2006. Water uptake by plant roots: II - Modelling of water transfer in the soil root-system with explicit account of flow within the root system - Comparison with experiments. *Plant and Soil*, **283**(1-2), 99–117.

Dukes, M.D., Zotarelli, L., & Morgan, K.T. 2010. Use of Irrigation Technologies for Vegetable Crops in Florida. *Agricultural Water Management*, **32**(3), 74–81.

Ehlers, W., & Goss, M. 2003. *Water dynamics in plant production.* Wallingford: CABI.

Feddes, R.A., Kowalik, P.J., & Zaradny, H. 1978. *Simulation of field water use and crop yield.* Wageningen: Centre for Agricultural Publishing and Documentation, W.

Gauly, M, Bollwein, H, Breves, G, Brugemann, K, Danicke, S, Das, G, Demeler, J, Hansen, H, Isselstein, J, Konig, S, Loholter, M, Martinsohn, M, Meyer, U, Potthoff, M, Sanker, C, Schroder, B, Wrage, N, Meibaum, B, von Samson-Himmelstjerna, G, Stinshoff, H, & Wrenzycki, C. 2013. Future consequences and challenges for dairy cow production systems arising from climate change in Central Europe - a review. *Animal*, **7**(5), 843–859.

Gong, Minggui, Tang, Ming, Chen, Hui, Zhang, Qiaoming, & Feng, Xinxin. 2013. Effects of two Glomus species on the growth and physiological performance of Sophora davidii seedlings under water stress. *New Forests*, **44**(3), 399–408.

Goudriaan, J. 1977. *Crop micrometeorology: a simulation study.* Tech. rept.

Halbertsma, J M, & Veerman, G J. 1994. *A new calculation procedure and simple set-up for the evaporation method to determine soil hydraulic functions.* Tech. rept.

Hunt, E R, Weber, J A, & Gates, D M. 1985a. Effects of Nitrate Application on Amaranthus-Powellii Wats. Changes in Photosynthesis, Growth-Rates, and Leaf-Area. *Plant physiology*, **79**(3), 609–613.

Hunt, E R, Weber, J A, & Gates, D M. 1985b. Effects of Nitrate Application on Amaranthus-Powellii Wats. Changes in Photosynthesis, Growth-Rates, and Leaf-Area. *Plant physiology*, **79**(3), 609–613.

Hyvönen, T. 2011. Impact of temperature and germination time on the success of a C4 weed in a C3 crop: Amaranthus retroflexus and spring barley. *Agricultural and Food Science*, **20**(November 2010), 183–190.

Irfan, Mohd, Hayat, Shamsul, Hayat, Qaiser, Afroz, Shaheena, & Ahmad, Aqil. 2010. Physiological and biochemical changes in plants under waterlogging. *Protoplasma*, **241**(1), 3–17.

Jalink, M.H., Laeven, M.P., & Ban Boschinga, W. 2000. *Winplaatsonderzoek Lieshout, Eindrapport, KOA 99.225.* Tech. rept. Kiwa N.V. Onderzoek en Advies, Nieuwegein.

Kacimov, A.R., & Obnosov, Yu.v. 2016. Tension-saturated and unsaturated flows fromline sources in subsurface irrigation: Riesenkampf's and Philip's solutions. *Water Resources Research*, 1–20.

Kaše, M., & Čatský, J. 1984. Maintenance and growth components of dark respiration rate in leaves of C3 and C4 plants as affected by leaf temperature. *Biologia Plantarum*, **26**(6), 461–470.

Kazumba, Shija, Gillerman, Leonid, Demalach, Yoel, & Oron, Gideon. 2010. Sustainable domestic effluent reuse via subsurface drip irrigation (SDI): Alfalfa as a perennial model crop. *Water Science and Technology*, **61**(3), 625–632.

Klein Tank, Albert, Beersma, Jules, Bessembinder, Janette, van den Hurk, Bart, & Lenderink, Geert. 2015. *KNMI klimaatscenario's voor Nederland '14.* Tech. rept. KNMI.

Klijn, Frans, ter Maat, Judith, & van Velzen, Emiel. 2011. *Zoetwatervoorziening in Nederland - landelijke analyse knelpunten in de 21e eeuw.* Tech. rept. Deltares.

Kroes, J G, van Dam, J C, Groenendijk, P, Hendricks, R F a, & Jacobs, C M J. 2008. *SWAP version 3.2: Theory description and user manual.* Tech. rept.

Kundzewicz, Zbigniew W., & Döll, Petra. 2009. Will groundwater ease freshwater stress under climate change? *Hydrological Sciences Journal*, **54**(4), 665–675.

Leij, F J, van Genuchten, M T, Yates, S R, & Russell, W B. 1992. RETC: a computer program for analyzing soil water retention and hydraulic conductivity data. *Pages 263–272 of: Indirect Methods for Estimating the Hydraulic Properties of Unsaturated Soils.*

Makkink, G F. 1957. Testing the Penman formula by means of lysimeters. *Journal of the Institution of Water Engineers*, **11**(3), 277—-288.

Moene, Arnold F., & Van Dam, Jos. C. 2014. *Transport in the Atmosphere-Vegetation-Soil Continuum*. Cambridge University Press.

Monteith, J L. 1965. *Evaporation and environment*.

Natuurlijk Kapitaal. 2016. *Icoonproject: Kringloop is doorbraak in papierindustrie*.

Nxawe, S., Ndakidemi, P.A., & Laubscher, C.P. 2010a. Possible effects of regulating hydroponic water temperature on plant growth, accumulation of nutrients and other metabolites. *African Journal of Biotechnology*, **9**(54), 9128–9134.

Nxawe, S., Ndakidemi, P.A., & Laubscher, C.P. 2010b. Possible effects of regulating hydroponic water temperature on plant growth, accumulation of nutrients and other metabolites. *African Journal of Biotechnology*, **9**(54), 9128–9134.

Odhiambo, L. O., & Irmak, S. 2015. Relative Evaporative Losses and Water Balance in Subsurface Drip and Center Pivot–Irrigated Soybean Fields. *Journal of Irrigation and Drainage Engineering*, **141**(11), 04015020.

Parry, Martin, Canziani, Osvaldo, Palutikof, Jean, van der Linden, Paul, & Hanson, Clair. 2007. *Climate Change 2007: impacts, adaptation and vulnerability: contribution of Working Group II to the fourth assessment report of the Intergovernmental Panel*. Cambridge University Press.

Penning de Vries, F W T, & van Laar, H H. 1982. Simulation of growth processes and the model BACROS. *Pages 114–135 of: Simulation of Plant Growth and Crop Production*. Wageningen: Simulation Monographs, Pudoc.

Phelan, P., Morgan, E. R., Rose, H., Grant, J., & O'Kiely, P. 2015. Predictions of future grazing season length for European dairy, beef and sheep farms based on regression with bioclimatic variables. *The Journal of Agricultural Science*, 1–17.

Planbureau voor de Leefomgeving. 2007. *Correctie formulering over overstromingsrisico Nederland in IPCC-rapport*.

Priestley, C.H.B., & Taylor, R.J. 1972. On the assessment of surface heat flux and evaporation using large-scale parameters. *Monthly weather review*, **100**(2), 81–92.

Raap, Johan. 2010. " Ook industrie opnemen in de waterketen ". *H2O*, **43**(23), 12–13.

Reyes-Cabrera, Joel, Zotarelli, Lincoln, Dukes, Michael D., Rowland, Diane L., & Sargent, Steven A. 2016. Soil moisture distribution under drip irrigation and seepage for potato production. *Agricultural Water Management*, **169**, 183–192.

Richards, L A. 1931. Capillary conduction of liquids through porous mediums. *Journal of Applied Physics*, **1**(5), 318–333.

Rijkswaterstaat. 1985. *Verbetering Zuid-Willemsvaart in Noord-Brabant - Principeplan*. Tech. rept. Rijkswaterstaat, management Noord-Brabant.

Ritchie, Joe T. 1972. Model for predicting evaporation from a row crop with incomplete cover. *Water Resources Research*, **8**(5), 1204–1213.

Schrama, E.J., & Jalink, M.H. 1998. *Winplaatsonderzoek Lieshout, Onderzoek Nuenen Groep, KOA 99.188*. Tech. rept. Kiwa N.V. Onderzoek en Advies, Nieuwegein.

Seligman, N G, & van Keulen, H. 1987. *Simulation of water use, nitrogen nutrition and growth of a spring wheat crop. Simulation.* Wageningen: Simulation Monographs Pudoc.

Shingaki-Wells, Rachel, Millar, A. Harvey, Whelan, James, & Narsai, Reena. 2014. What happens to plant mitochondria under low oxygen? An omics review of the responses to low oxygen and reoxygenation. *Plant, Cell and Environment*, **37**(10), 2260–2277.

Šimůnek, Jiří, & Hopmans, Jan W. 2009. Modeling compensated root water and nutrient uptake. *Ecological Modelling*, **220**(4), 505–521.

Stichting voor bodemkartering. 1981. *Bodemkaart van Nederland; Schaal 1:50000; Toelichting bij kaartblad 51 Oost Eindhoven.* Tech. rept. Stichting voor Bodemkartering, Wageningen.

Stuyt, L.C.P.M., van der Bolt, F.J.E., Snellen, W.B., Groenendijk, P., Schipper, P.N.M., & Harmsen, J. 2012. *Meer water met regelbare drainage?* Tech. rept.

Terink, W, van Bakel, P.J.T., van den Eertwegh, G.A.P.H., & Droogers, P. 2013. *Klimaatadaptieve Drainage- Samenvatting resultaten fase 2.* Tech. rept.

Vadez, Vincent. 2014. Root hydraulics: The forgotten side of roots in drought adaptation. *Field Crops Research*, **165**, 15–24.

van Bakel, P.J.T., van Boekel, E.M.P.M., & Noij, I.G.A.M. 2008. *Modelonderzoek naar effecten van conventionele en samengestelde, peilgestuurde drainage op de hydrologie en nutriëntenbelasting.* Tech. rept. Alterra, Wageningen.

van Dobben, W H. 1962. Influence of temperature and light conditions on dry-matter distribution, development rate and yield in arable crops. *Netherlands Journal of Agricultural Science*, **10**, 377–389.

van Genuchten, M. Th. 1980. A Closed-form Equation for Predicting the Hydraulic Conductivity of Unsaturated Soils. *Soil Science Society of America Journal*, **44**(5), 892.

Vogel, T., Van Genuchten, M. Th, & Cislerova, M. 2000. Effect of the shape of the soil hydraulic functions near saturation on variably-saturated flow predictions. *Advances in Water Resources*, **24**(2), 133–144.

Von Hoyningen-Hüne, J. 1981. *Die Interception des Niederschlags in landwirtschaftlichen Beständen.* Arbeitsbericht Deutscher Verband für Wasserwirtschaft und Kulturbau, DVWK.

Wahid, A., Gelani, S., Ashraf, M., & Foolad, M. R. 2007. Heat tolerance in plants: An overview. *Environmental and Experimental Botany*, **61**(3), 199–223.

Wang, Xiao, Huang, Mei, Zhou, Qin, Cai, Jian, Dai, Tingbo, Cao, Weixing, & Jiang, Dong. 2016. Physiological and proteomic mechanisms of waterlogging priming improves tolerance to waterlogging stress in wheat (Triticum aestivum L.). *Environmental and Experimental Botany*, **132**, 175–182.

Wendroth, Ole, Ehlers, W., Kage, H., Hopmans, J. W., Halbertsma, J., & Wösten, J. H. M. 1993. Reevaluation of the evaporation method for Determining hydraulic functions in unsaturated Soils. *Soil Science Society of America Journal*, **57**(6), 1436–1443.

Wind, G P. 1968. Capillary conductivity data estimated by a simple method. *Water in the unsaturated zone*, **1**, 181–191.

Wösten, J. H M, Veerman, G.J, DeGroot, W.J.M, & Stolte, J. 2001. Waterretentie- en doorlatendheidskarakteristieken van boven- en ondergronden in Nederland: de Staringreeks. *Alterra Rapport*, **153**, 86.

Zhao, M., Peng, C., Xiang, W., Deng, X., Tian, D., Zhou, X., Yu, G., He, H., & Zhao, Z. 2013. Plant phenological modeling and its application in global climate change research: Overview and future challenges. *Environmental Reviews*, **21**(1).

Appendix A

Evaporation method: De-aeration tensiometers and pressure transducers

For the de-aeration of the tensiometers fifty conventional tensiometers were placed in a container with water. These tensiometers can measure heads from -800 to 0 cm. The tap of the tensiometers was placed in the way as is shown in figure 4.4, so water can float inside the tube of the tensiometer. The container was placed under a glass bell, which was connected to a vacuum plunger. The vacuum plunger caused an underpressure of -900 mbar. The whole installation was placed on a vibrating plate. The vacuum and the vibration were used to remove air out of the tensiometers and out of the water. After a few hours, the vacuum plunger and the fibration plate were turned off. The tensiometers were now expected to be fully saturated with anoxic water. Tensiometers should be permeable when the ceramic cup is wet and they should be impermeable when the ceramic cup is dry. To test if the tensiometers were not leak, the tensiometers were one by one connected to a tube which was connected to the vacuum plunger. An air bubble was created by shortly opening the tap of the tensiometer. At first the tensiometer was kept into the water. By this water would flow into the tensiometer, sucked by the vacuum plunger. Then the tensiometer was put outside the water and is dried by a tissue. The dry tensiometer should now be impermeable. So despite of the vacuum plunger, no air should be sucked inside the tensiometer. This was checked by the air bubble, which should not move now the tensiometer was dry. 36 of the tensiometers which were not leak were used in the evaporation method. The tap of these tensiometers was closed under water, so no air was located inside the tensiometers and the tubes.

For each soil sample, four tested tensiometers were placed in a measuring cup with water. Nine evaporation installations were used, for every soil sample one. The installations contain a balance and four pressure transducers at the same heights as holes in the PVC ring, when the ring was placed on the balance. The pressure transducers were connected to a computer. For each installation the four tensiometers were connected to the pressure transducers. The tap above the pressure transducers was opened. A syringe filled with anoxic water was connected to one of the tensiometers and the tap was placed in such a way that the syringe and the pressure transducer were connected. The pressure transducer was connected by a tube to the measuring cup. It is important that the tap on top of the pressure transducer was open, because pressure transducers cannot withstand overpressure. The syringe was carefully emp-

tied until there was no air anymore inside the pressure transducer. Then the tap of the tensiometer was placed in such way that the tensiometer and the pressure transducer were only connected with each other. The syringe and the tube on top of the pressure transducer were removed and the other tensiometers and pressure transducers were installed in the same way.

Appendix B

Filtering measurements for Wind procedure

In the file *E.Filter V6.4*, first the switch between winter and summer time was checked. The next step was to add the mean volumetric water content per time step. This mean volumetric water content was calculated by:

$$\overline{\theta}(t) = m(t) - m_{end} + m_{bowl,wet} - m_{bowl,dry} \tag{B.1}$$

In which $\overline{\theta}(t)$ is the mean volumetric water content at time is t, $m(t)$ is the weight measured by the balance at time is t, m_{end} is the weight of the last measurement measured by the balance, $m_{bowl,wet}$ is the weight of the sample with the bowl just before the sample was put into the oven and $m_{bowl,dry}$ is the weight of the sample with the bowl after it was put into the oven.

After adding $\overline{\theta}(t)$ to the data, faulty begin values were discarded. These values originate from measurements when the sample was not yet installed or the water inside the sample was not yet in equilibrium. Now for each sample, possible ending points of the data were decided. The possible ending points were chosen just before a tensiometer failed. Therefore such an ending point was the latest point with that tensiometer included. Care was taken that the measurements of the including tensiometers were all stable, without quick changes in the measured head. Ending points were points on which at least two tensiometers are still working, because only then the analysis could be completed. For every ending point all possible variations in tensiometers included and excluded were investigated. Here minimal two tensiometers should be included.

Hereafter the bandwidth, the minimum change in head over the depth and the lowest time step used were specified. Then the filter software splits the measurements in three categories; measurements which could be used for both the determination of both $\theta(h)$ and $K(\theta)$, measurements which could only be used for the determination of $\theta(h)$ and measurements which could not be used. For measurements used for both $\theta(h)$ and $K(\theta)$, all valid tensiometers should have decreasing values and all head values should be within the bandwidth. Measurements used for $K(\theta)$ should also meet the specified change in head over depth and the specified lowest time step. The division between measurements for the $\theta(h)$ and $K(\theta)$ relationship was made because measurements for the $K(\theta)$ relationship needed to have changes in head over depth of minimal 1, otherwise negative K values would be obtained by using Darcys formula. Measurements which do not fulfil this criterion could still be used for the $\theta(h)$ relationship. For all possible variations in ending points and tensiometers included per sample, the amount of measurements used for both $\theta(h)$ and $K(\theta)$ were viewed. This should be maximal 1000, because maximum 1000 measurements could be used in the next step.

Besides, at least 30 measurements should be used for $K(\theta)$, since 30 is the minimal amount of measurements needed to obtain the $K(\theta)$ relationship. By changing the band width, the minimum change in head over depth and the minimum time step, the amount of measurements for the determination of each relation could be controlled.

Appendix C

Calculations extra heat flux SWAP

Without extra heat flux, the finite difference used by SWAP reads:

$$C_i^{j+0.5} * \left(T_i^{j+1} - T_i^j\right) =$$
$$\frac{\Delta t^j}{\Delta z_i}\left[\lambda_{i+0.5}^{j+0.5} \cdot \left(\frac{T_{i+1}^{j+1} - T_i^{j+1}}{\Delta z_l}\right) - \lambda_{i-0.5}^{j+0.5} \cdot \left(\frac{T_i^{j+1} - T_{i-1}^{j+1}}{\Delta z_l}\right)\right] \tag{C.1}$$

In here i is the discretization in space and j is the discretization in time. With the extra heat flux implemented, the finite difference function becomes:

$$C_i^{j+0.5} * \left(T_i^{j+1} - T_i^j\right) =$$
$$\frac{\Delta t^j}{\Delta z_i}\left[\lambda_{i+0.5}^{j+0.5} * \left(\frac{T_{i+1}^{j+1} - T_i^{j+1}}{\Delta z_l}\right) - \lambda_{i-0.5}^{j+0.5} * \left(\frac{T_i^{j+1} - T_{i-1}^{j+1}}{\Delta z_l}\right)\right] + S_{heat,i}^j \tag{C.2}$$

This function can be rewritten as:

$$-\frac{\Delta t^j}{\Delta z_i \Delta z_u}\lambda_{i-0.5}^{j+0.5} * T_{i-1}^{j+1} + \left[C_i^{j+0.5} + \frac{\Delta t^j}{\Delta z_i \Delta z_u}\lambda_{i-0.5}^{j+0.5} + \frac{\Delta t^j}{\Delta z_i \Delta z_l}\lambda_{i+0.5}^{j+0.5}\right] T_i^{j+1}$$
$$-\frac{\Delta t^j}{\Delta z_i \Delta z_l}\lambda_{i+0.5}^{j+0.5} * T_{i+1}^{j+1} = C_{i+1}^{j+0.5} * T_i^j + S_{heat,i}^j \tag{C.3}$$

The finite difference with extra heat flux can be expressed in a tri-diagional matrix:

$$M = \begin{bmatrix} \beta_1 & \gamma_1 & & & & & \\ \alpha_2 & \beta_2 & \gamma_2 & a & a & a & a \\ & \alpha_3 & \beta_3 & \gamma_3 & & & \\ & & & & & & \\ & & & & \alpha_{n-1} & \beta_{n-1} & \gamma_{n-1} \\ & & & & & \alpha_n & \beta_n \end{bmatrix} \cdot \begin{bmatrix} T_1^{j+1} \\ T_2^{j+1} \\ T_3^{j+1} \\ \\ T_{n-1}^{j+1} \\ T_n^{j+1} \end{bmatrix} = \begin{bmatrix} f_1 \\ f_2 \\ f_3 \\ \\ f_{n-1} \\ f_n \end{bmatrix} \tag{C.4}$$

In here

$$\alpha_i = -\frac{\Delta t^j}{\Delta z_i \Delta z_u}\lambda_{i-0.5}^{j+0.5}$$
$$\beta_i = C_i^{j+0.5} + \frac{\Delta t^j}{\Delta z_i \Delta z_u}\lambda_{i-0.5}^{j+0.5} + \frac{\Delta t^j}{\Delta z_i \Delta z_l}\lambda_{i+0.5}^{j+0.5}$$

$$\gamma_i = \frac{\Delta t^j}{\Delta z_i \Delta z_l} \lambda_{i+0.5}^{j+0.5}$$

$$f_i = C_i^{j+0.5} * T_i^j$$

An exception is when i is the node of the drain. Then the extra heat flux is implemented in f_i :

$$f_i = C_i^{j+0.5} * T_i^j + S_{heat,i}^j$$

With

$$S_{heat,i}^j = q_{inf} * \left(T_{inf}^j - T_i^j\right) * C_i^j * \frac{1}{\Delta z_i}$$

Appendix D

Linear regression with soil temperature measurements

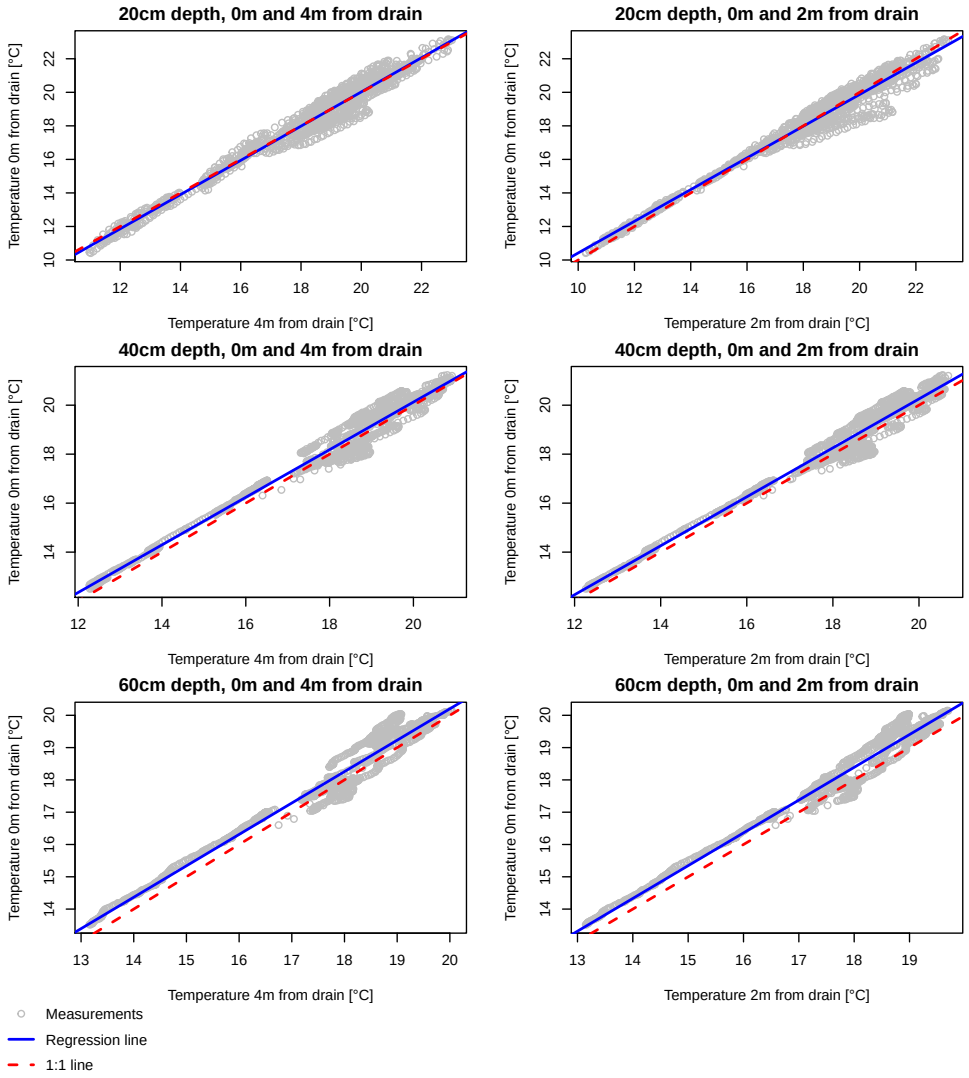

Figure D.1: The plots of the linear regression. In every plot two soil temperature measurements taken at the same depth are plotted against each other. The measurements in one plot are taken at a horizontal distance of 0m, 2m or 4m from the drain.